International Journal of Coal Geology 228 (2020) 103555

Contents lists available at ScienceDirect

International Journal of Coal Geology

journal homepage: www.elsevier.com/locate/coal

Petrographic and organic geochemical study of the Eocene Kosd Formation (northern Pannonian Basin): Implications for paleoenvironment and hydrocarbon source potential

Sándor Körmös[a,b,*], Achim Bechtel[b], Reinhard F. Sachsenhofer[b], Balázs Géza Radovics[c], Katalin Milota[c], Félix Schubert[a]

[a] University of Szeged, Department of Mineralogy, Geochemistry and Petrology, Egyetem u. 2, H-6722 Szeged, Hungary
[b] Montanuniversität Leoben, Petroleum Geology, Peter-Tunner-str. 5, A-8700 Leoben, Austria
[c] MOL Plc, Október huszonharmadika u. 18, H-1117 Budapest, Hungary

ARTICLE INFO

Keywords:
Eocene Kosd Formation
High volatile bituminous coal
Hungarian Palaeogene Basin
Organic geochemistry
Organic petrology

ABSTRACT

The Eocene Kosd Formation forms part of the Hungarian Palaeogene Basin. The coal measure of this formation was investigated using an 18 m drill core from borehole W–1. Petrographic and organic geochemical investigations (Rock-Eval pyrolysis, biomarker analysis) were performed in order to characterize the depositional environment, to determine the source of the organic matter within, and to assess the hydrocarbon generative potential.

The presence of marine fossils, high TOC/S ratios and ash yields show that the deposition of the coal measure occurred in a marine delta with individual coal layers accumulating in low-lying, rheotrophic mires. The distribution of land plant-derived biomarkers demonstrates that the peat-forming vegetation was dominated by angiosperms, but the relative contribution of gymnosperms varied through time. In addition to land plants, algae and aquatic macrophytes contributed to the biomass. This dense vegetation established a CO_2-limited environment forcing aquatic plants to utilise HCO_3^- during photosynthesis. The marine environment, as well as the predominance of carbonate rocks in the hinterland, caused slightly alkaline conditions, which, together with reduced oxygen availability, stimulated sulphate-reducing bacterial activity and the microbial degradation of plant remains. Consequently, Kosd Formation coal is very rich in sulphur (up to 8.8%). Moreover, the coal contains vitrinite with a strong orange-brown fluorescence colour and swells strongly during pyrolysis. These features are typical for coals with marine influences.

Vitrinite reflectance, Tmax, and biomarker proxies indicate that the organic matter is thermally mature and that the Kosd coal reached the high volatile bituminous rank in the deep borehole (~2.6 km depth). Rock-Eval parameters imply that the coal is gas- and oil-prone and reached the maturity threshold critical for first gas generation and the onset of oil expulsion.

1. Introduction

During the Eocene, the Mesozoic Tethys Ocean decayed into a series of intercontinental seas (Rögl, 1999). This new configuration of land and sea areas modified oceanic circulation and climate (Popov et al., 2001). In the Late Eocene, Europe formed an archipelago and was enclosed by a subtropical sea, where variations in sea level significantly affected the distribution of depositional environments (Sachsenhofer et al., 2018).

The Hungarian and Slovenian Palaeogene Basin is a predecessor of the Pannonian Basin (Tari et al., 1993). During the Eocene, sedimentation in this basin was characterized by a generally transgressive nature, where depocenters shifted northeastwards through time (Báldi and Báldi-Beke, 1985; Kováč et al., 2016). Hence, coal formation started earlier in the area of the present-day Transdanubian Mountains (the Middle Eocene Dorog Coal Formation) than in the North Hungarian Mountains (the Upper Eocene coal-bearing Kosd Formation; Figs. 1, 2; Báldi-Beke, 2003a, 2003b; Gidai, 1978; Hámor-Vidó and Hámor, 2007). The Kosd Formation includes economic coal seams (Gidai, 1978). The Kosd coalfield (location is shown in Fig. 1) is registered in the national coal cadastre of Hungary (MGSH – Mining and Geological Survey of Hungary, 2019), however, mining of this sub-

* Corresponding author at: University of Szeged, Department of Mineralogy, Geochemistry and Petrology, Egyetem u. 2, H-6722 Szeged, Hungary.
E-mail address: sandor.kormos@geo.u-szeged.hu (S. Körmös).

https://doi.org/10.1016/j.coal.2020.103555
Received 2 April 2020; Received in revised form 1 July 2020; Accepted 5 July 2020
Available online 15 July 2020

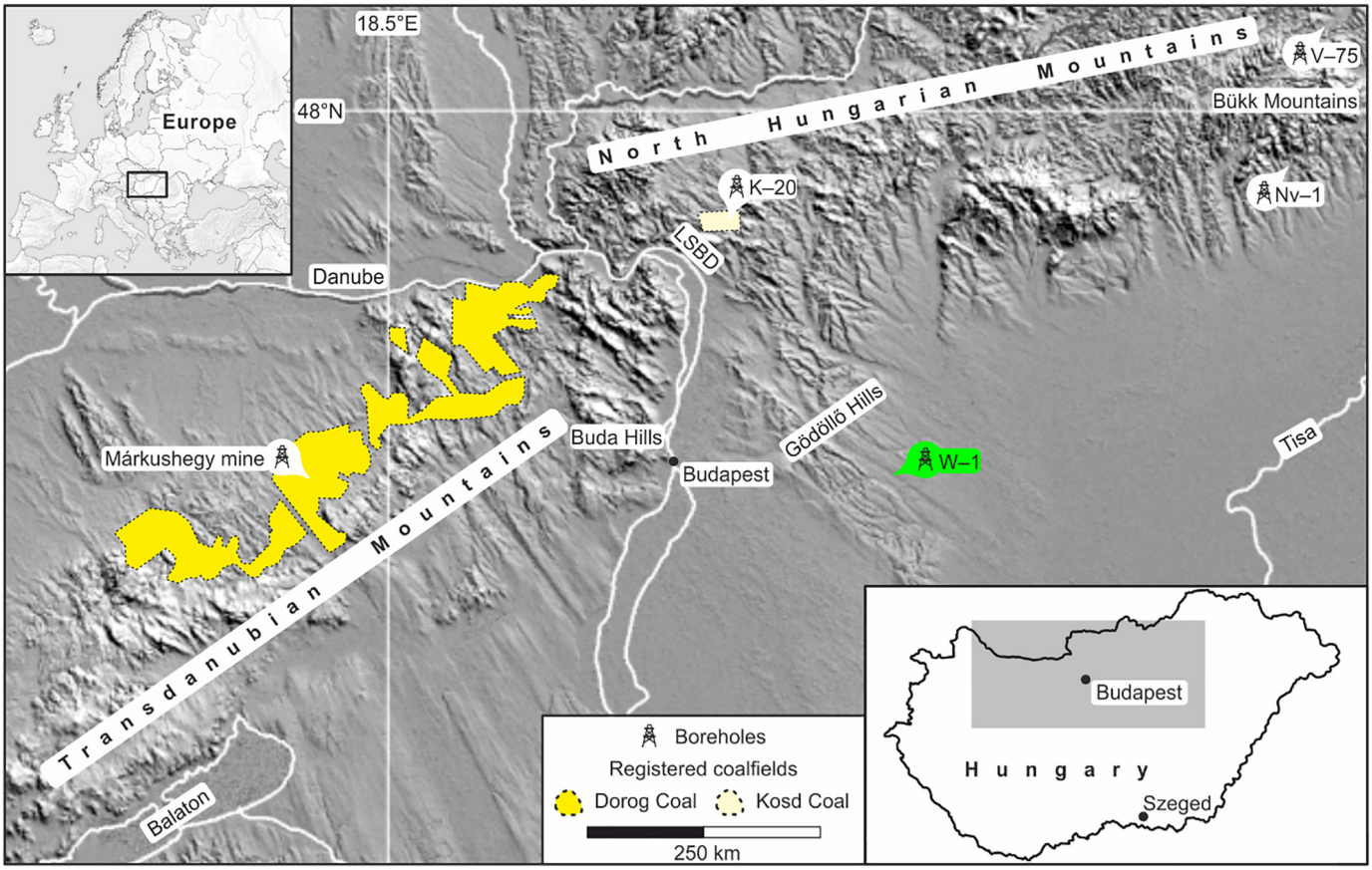

Fig. 1. Location of registered Eocene sub-bituminous coalfields: Kosd–20 (K – 20), Varbó–75 (V–75), Noszvaj–1 (Nv–1), and the investigated W–1 boreholes. Modified following the digital elevation model and digital coal cadastre of Hungary (Horváth et al., 2005; MGSH – Mining and Geological Survey of Hungary, 2019). LSBD – Left Side Blocks of Danube.

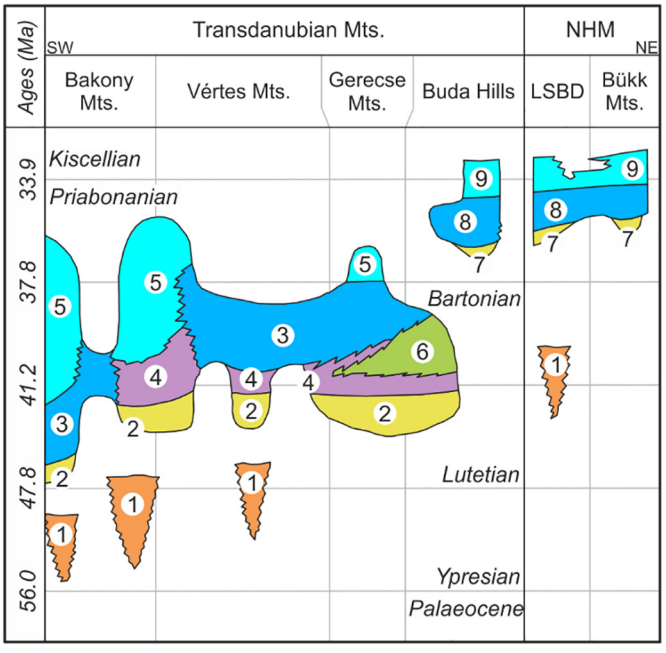

Fig. 2. Eocene lithostratigraphy across the North-Hungarian range (modified after Kercsmár et al., 2015; Less, 2015 oral communication). NHM – North Hungarian Mountains and LSBD – Left Side Blocks of Danube. 1 – Gánt Bauxite Formation, 2 – Dorog Coal Formation, 3 – Szőc Limestone Formation, 4 – Csolnok Formation, 5 – Padrag Marl Formation, 6 – Tokod Formation, 7 – Kosd Formation, 8 – Szépvölgy Limestone Formation, 9 – Buda Marl Formation.

bituminous coal ended in the 1930s (Némedi Varga, 2010).

Bechtel et al. (2007) performed an exhaustive geochemical study on the Middle Eocene Dorog Coal finding that the seam originates from a topogenous mire and evolved within a peneplane coastal area covered with eutrophic swamps. The peat-forming vegetation at the time was predominated by angiosperms, which is characteristic of Eocene coals throughout central Europe (Bechtel et al., 2008). In contrast, factors controlling the depositional environment and coal facies of the Upper Eocene Kosd coal have not previously been investigated.

Maceral composition, petrography-based facies indicators and biomarker analysis became essential tools during the last decades for the reconstruction of paleoenvironments and peat-forming floral changes (e.g. Bechtel et al., 2003, 2007; Gross et al., 2015; Sachsenhofer et al., 2010). Additionally, the stable carbon isotope composition of individual biological markers allows the identification of specific sources (Hayes et al., 1987). Primary producers fix inorganic carbon through photosynthesis, which leads to specific fractionation of carbon isotopes (Diefendorf and Freimuth, 2017; Holtvoeth et al., 2019). Ficken et al. (1998) found that accumulating organic matter experiences rapid microbial degradation and associated diagenetic changes in the top few centimetres of sediment. Other studies, however, have reported no significant changes in $\delta^{13}C$ during early diagenesis (Li et al., 2017, and references therein). Thermal maturation of organic matter may nonetheless affect the carbon isotope composition (Bjorøy et al., 1992; Clayton, 1991; Rooney et al., 1998). The degree of isotope fractionation depends on the temperature, but the effect is limited to a range of 2‰ as maturity progresses (Clayton, 1991; Schoell, 1984). Therefore, biologically controlled isotope compositions can be used to identify precursor sources after diagenesis (e.g. Collister et al., 1994; Freeman et al., 1990; Rieley et al., 1991).

The current study is based on samples from borehole W–1, located about 50 km SE from the abandoned Kosd coalfield (Fig. 1), which drilled the Eocene succession beneath potential Oligocene hydrocarbon source rocks. Whereas the Oligocene source rocks have been investigated by several authors (e.g. Badics and Vető, 2012; Bechtel et al., 2012; Milota et al., 1995; Sachsenhofer et al., 2018), the Eocene Kosd Formation remained largely uninvestigated.

The aims of this study are therefore to enhance understanding of the depositional environment and organic matter sources in this formation, and to estimate the hydrocarbon potential of deep Eocene Kosd coal. To achieve this goal, organic petrological and organic geochemical analyses were performed.

2. Geological setting

A series of sub-bituminous coalfields of Middle Eocene Dorog Coal Formation occur along the Transdanubian Mountains (Hámor-Vidó and Hámor, 2007; Bechtel et al., 2007). Eocene coal in the North Hungarian Mountains belongs to the Upper Eocene Kosd Formation (Fig. 1; Gidai, 1978; Báldi-Beke, 2003a, 2003b). The diachronous development of depocenters followed the gradual northeastward trend of the Eocene transgression (Báldi and Báldi-Beke, 1985). In the western part of the Transdanubian Mountains, the initial transgression took place during the early Lutetian. The next transgression flooded the entire Transdanubian Range during the late Lutetian (the Dorog Coal Formation; Fig. 2). In contrast, for the eastern part of the Transdanubian Mountains and the North Hungarian Mountains, the transgression occurred during the Bartonian and Priabonian (the Kosd Formation; Fig. 2; Báldi-Beke, 2003a, 2003b; Kercsmár et al., 2015; Kováč et al., 2016).

The Kosd Formation crops out in small areas throughout the Buda Hills, the Left Side Blocks of Danube and the Bükk Mountains. In the subsurface, it extends towards the south into the Gödöllő Hills (Fig. 1), where it was encountered by several boreholes (e.g. Bauer et al., 2016; Palotai and Csontos, 2010).

The Kosd Formation unconformably overlies the Mesozoic basement, which belongs to different mega-units. In the Buda Hills and the Left Side Blocks of Danube (Transdanubian Range Unit) the basement is represented by Ladinian to Norian platform carbonates (e.g. the Budaörs Dolomite Formation; the Dachstein Limestone Formation), and cherty basinal carbonates (e.g. the Mátyáshegy Formation; Haas and Kovács, 2012). In the Bükk Mountains (Bükk Unit), in addition to Ladinian to Norian platform carbonates (e.g. the Berva Limestone Formation; the Kisfennsík Limestone Formation) and basinal carbonates (the Felsőtárkány Limestone Formation), a deep marine Middle to Upper Jurassic sedimentary succession, with debris flows and turbidites, are present (the Mónosbél Group; Pelikán, 2005). The Mesozoic strata were uplifted during the Late Cretaceous and as a consequence of the subaerial exposure intense karstification occurred (Haas and Kovács, 2012).

Depending on the palaeotopography of the karst surface, the thickness of the Kosd Formation varies considerably and reaches 244 m in borehole Noszvaj–1 (Nv–1; the location is shown in Fig. 1; Less, 2005). The Kosd Formation was described in detail in two wells (Kosd–20 [K − 20]; Varbó–75 [V–75]; Fig. 1) by Gidai (1978) and Less (2005). In both wells, the Kosd Formation is characterized by two different sedimentary facies. The lower facies contains fossil- and carbonate-free variegated clay with different amounts of rock debris, deposited in a terrestrial environment. The overlying sediments include claystone, siltstone with varying carbonate content, marl and thin coal layers (Gidai, 1978; Less, 2005). The thickness of the lower and upper sedimentary sequences is 63 and 12 m, respectively, at V–75 well (Less, 2005) and 9 and 123 m, respectively, at K–20 well (Gidai, 1978). The coal is intercalated into calcareous claystone and marl at V–75 and K–20 wells, respectively, whereas the direct underlying sediments are characterized by varicoloured clay with carbonate debris. The overlying sediments grade into Miliolina-bearing calcareous marl. Gidai (1978) and Less (2005) noted an upward transition from a freshwater environment, indicated by gastropods (*Melanopsis* sp.) to a shallow marine, lagoonal environment marked by the presence of nannoplankton (*Isthmolithus recurves*) and foraminifers (*Quinqueloculina*, *Nummulites* sp.). Moreover, a proximal coastal environment is supported by mangrove vegetation, represented by Nypa palm pollens (Kvaček, 2010, and references therein; Rákosi, 1978). Coaly layers were noted by Gidai (1978) and Less (2005) in boreholes K–20 and V–75, but were not investigated in detail.

The Kosd Formation grades upward into shallow marine platform carbonates of the Szépvölgy Limestone Formation (Fig. 2). The presence of the corallinacean algae and the frequently-occurring monospecific *Nummulites fabianii* indicate deposition on the inner shelf, while a diverse fauna including orthophragminas in the upper part of the formation, marks a transition to an outer shelf environment during the deposition of Szépvölgy Limestone (Less, 2005). Continuing basin subsidence caused deposition of the shallow bathyal Buda Marl Formation, in low-oxic environments across the Eocene-Oligocene transition (Ozsvárt et al., 2016). The Tard Clay Formation accumulated in oxygen-depleted conditions (Bechtel et al., 2012; Ozsvárt et al., 2016), and the Kiscell Clay Formation was deposited in a more oxygenated environment (Bechtel et al., 2012). A sequence of siliciclastic and carbonate platform sediments terminates the Palaeogene succession, which is followed by thick Neogene deposits (Less, 2005; Kercsmár et al., 2015).

The coal measures of the Kosd Formation in the former Kosd coalfield (Fig. 1) are 5 to 32 m thick and include three seams (Kubacska, 1925; Gidai, 1978; Némedi Varga, 2010). The lower seam is 0.5 to 2.5 m thick and was exploited between 1904 and 1931 via an underground mine approximately 130 m below the surface. The coal reaches the sub-bituminous stage in the shallow mine. Based on contemporary data (Papp, 1913), the coal includes 3–4 wt% moisture and the ash yield varies from 6 to 20 wt%. The elemental composition of the coal is 56–67 wt% carbon, 4–6 wt% hydrogen, 1 wt% nitrogen and 5–6 wt% sulphur (Papp, 1913). According to Némedi Varga (2010), the average calorific value is 19 MJ/kg and the potential reserves were estimated as 15 Mt.

3. Samples and analytical methods

3.1. Samples

Borehole W–1, drilled in the early 2000s in the southern part of the Gödöllő Hills by MOL Plc. (Fig. 1), penetrated the Kosd Formation from 2415 m to 2791 m. A drill core, representing the upper section of the coal measures in the Kosd Formation, was recovered from 2587 m to 2605 m. In total, 35 samples (Table 1) were obtained from this drill core, each of them was selected based on lithological differences and is representative of a 20 cm interval. In order to avoid contamination, about 0.5 cm of the outer rim of each core was removed. Moreover, to prevent outlier readings, samples containing pyrite aggregates or nodules were not selected during sample collection. Pyrite crystals in the macroscopic range were hand-picked from the samples prior to pulverization.

3.2. Petrographic analysis

Fifteen core samples, including all coal and coaly shale samples as well as selected mudstone samples, were prepared as whole-rock polished blocks for maceral analyses. Each sample was cut perpendicular to the bedding plane, embedded in epoxy resin and polished according to standard procedures (ASTM International, 2015). Organic matter was identified by reflected white- and UV-fluorescent light microscopy using a Leica DM4P microscope equipped with a 50× oil-immersion objective and a point counter equipped with an OptiScan fully automated scanning stage. Maceral analyses were performed using a single

Table 1
Bulk geochemical parameters of samples from the Kosd Formation.

ID	Depth	Lithotype	TIC	TOC	CEq	TS	Ash yield	TOC/TS	S1	S2	HI	BI	QI	PI	Tmax
#	[m; MD]		[wt%, db]						[mg HC/g rock]		[mg HC/g TOC]				[°C]
1	2587.10	siltstone	0.6	0.6	4.9	2.5	–	0.2	0.1	0.3	51	–	–	0.30	441
2	2587.75	siltstone	2.5	0.5	20.5	2.1	–	0.2	0.1	0.4	75	–	–	0.24	446
3	2588.00	siltstone	1.3	0.6	10.9	2.4	–	0.2	0.2	0.4	63	–	–	0.31	446
4	2589.20	siltstone	1.3	0.7	10.4	2.8	–	0.3	0.3	0.5	71	–	–	0.35	445
5	2590.00	coaly shale	0.8	29.5	6.8	4.0	59.4	7.3	10.0	71.9	243	34	277	0.12	441
6	2590.20	claystone	–	7.2	–	1.6	–	4.6	2.5	20.9	289	–	–	0.11	443
7	2591.00	siltstone	0.9	1.2	7.5	2.9	–	0.4	0.6	1.0	80	–	–	0.39	443
8	2591.80	siltstone	2.8	0.5	23.6	2.3	–	0.2	0.3	0.5	102	–	–	0.37	439
9	2592.20	siltstone	4.3	0.5	36.1	1.7	–	0.3	0.1	0.3	62	–	–	0.32	443
10	2593.00	siltstone	0.8	0.6	6.6	1.4	–	0.4	0.2	0.3	60	–	–	0.31	446
11	2593.70	siltstone	2.3	0.6	18.9	2.5	–	0.3	0.3	0.4	65	–	–	0.39	446
12	2594.40	siltstone	0.9	0.4	7.3	2.5	–	0.2	0.1	0.1	36	–	–	0.33	439
13	2594.55	coaly shale	0.7	12.7	5.7	3.5	77.9	3.6	3.8	31.9	251	30	280	0.11	441
14	2594.92	siltstone	0.9	1.5	7.8	2.6	–	0.6	0.7	1.0	68	–	–	0.40	439
15	2596.80	siltstone	0.9	0.5	7.8	1.7	–	0.3	0.5	0.3	66	–	–	0.61	446
16	2597.00	siltstone	0.9	0.5	7.6	2.4	–	0.2	0.1	0.2	40	–	–	0.38	438
17	2597.40	siltstone	1.0	0.8	8.4	3.2	–	0.3	0.3	0.5	64	–	–	0.36	447
18	2598.30	siltstone	0.8	0.9	6.3	2.4	–	0.4	0.6	0.6	65	–	–	0.51	437
19	2598.50	siltstone	0.6	0.8	5.2	2.5	–	0.3	0.6	0.5	54	–	–	0.56	432
20	2599.00	siltstone	0.1	1.0	0.5	3.2	–	0.3	0.4	0.4	39	–	–	0.47	431
21	2599.90	coal	0.4	78.4	3.6	3.4	5.8	23.0	23.4	186.3	238	30	267	0.11	443
22	2600.00	claystone	–	2.9	–	4.8	–	0.6	1.1	3.0	103	–	–	0.27	443
23	2600.60	claystone	0.1	2.9	1.0	3.0	–	1.0	1.5	2.9	101	–	–	0.34	445
24	2600.95	coal	–	45.7	–	8.8	32.1	5.2	14.6	133.1	291	32	323	0.10	441
25	2601.00	siltstone	–	3.8	–	4.5	–	0.9	1.8	6.6	171	–	–	0.22	448
26	2601.20	coaly shale	0.3	25.0	2.7	5.9	62.0	4.2	9.3	66.1	264	37	301	0.12	440
27	2601.40	siltstone	1.1	3.0	9.3	4.7	–	0.6	1.1	4.9	165	–	–	0.19	446
28	2602.00	coaly shale	–	21.8	–	4.9	66.2	4.5	6.6	53.8	247	30	277	0.11	438
29	2602.40	siltstone	1.4	1.0	11.9	3.4	–	0.3	0.9	0.8	82	–	–	0.52	444
30	2602.60	siltstone	1.1	1.0	8.8	3.1	–	0.3	0.9	0.7	71	–	–	0.55	441
31	2603.30	siltstone	1.1	0.7	9.1	3.0	–	0.2	0.5	0.6	90	–	–	0.47	441
32	2603.50	siltstone	1.8	0.7	15.4	3.1	–	0.2	0.5	0.7	97	–	–	0.41	442
33	2604.10	siltstone	3.5	0.8	29.3	2.1	–	0.4	0.4	0.7	92	–	–	0.38	443
34	2604.90	coal	1.1	57.2	9.0	3.4	30.5	16.6	17.2	130.8	229	30	259	0.12	444
35	2605.00	claystone	1.1	0.8	9.4	2.6	–	0.3	0.5	0.9	107	–	–	0.38	444

MD – measured depth; db – dry basis; TIC – total inorganic carbon content, TOC – total organic carbon content, CEq – calcite equivalent, TS – sulphur content, TOC/TS – ratio of total organic carbon versus total sulphur content, S1 – free hydrocarbons, S2 – hydrocarbons generated during Rock-Eval pyrolysis, HI – hydrogen index, BI – bitumen index, QI – quality index, PI – production index, Tmax – temperature of maximum hydrocarbon generation.

scan method (Taylor et al., 1998) considering at least 1500 individual points to assess the minimum 500 counts of macerals. The terminology and classification of macerals used in this study are based on the ICCP system (ICCP, 1998, 2001; Pickel et al., 2017).

Mean random reflectance (%Rr) of telovitrinite was measured according to the methods of Taylor et al. (1998), and was performed under monochromatic (546 nm) light using an Olympus BX41 microscope equipped with a 50× oil-immersion objective and optical standards of Buehler Ltd. Reflectance values were processed by image analysis (Taylor et al., 1998).

3.3. Organic geochemical analysis

Powdered rock samples were analysed in duplicate for total sulphur (TS) and total carbon (TC) contents using an ELTRA Helios CS-580A analyser. Samples pre-treated by hot and diluted H_3PO_4 were used to determine total organic carbon (TOC) content. Total inorganic carbon (TIC = TC – TOC) was used to calculate calcite equivalent (CEq) percentages (CEq = TIC × 8.34 [%]). Ash yields were determined according to standard procedures (ASTM International, 2018).

Pyrolysis was carried out in duplicate using a Rock-Eval 6 instrument (Lafargue et al., 1998). The S1 and S2 peaks were recorded in order to determine the quantities of free (S1 [mg HC/g rock]) and generated hydrocarbons (S2 [mg HC/g rock]). The temperature of maximum hydrocarbon generation (Tmax [°C]) was recorded and used as a maturity indicator. Derived parameters were also calculated, such as the hydrogen index (HI; HI = S2 × 100/TOC [mg HC/g TOC]), production index (PI; PI = S1/(S1 + S2) [−]; Espitalié et al., 1977), bitumen index (BI; BI = S1 × 100/TOC [mg HC/g TOC]; Killops et al., 1998) and quality index (QI; QI = (S1 + S2) × 100/TOC [mg HC/g TOC]; Pepper and Corvi, 1995).

Based on the results of Rock-Eval pyrolysis and the diverse lithologies observed, ten samples (#20 to #29) representing the depth interval between 2599.0 and 2602.4 m were chosen for solvent extraction. The upper- and lowermost samples represent typical low-TOC intercalating lithologies, whereas the others are coaly shale and coal samples together with their adjacent sediments.

Representative portions of powdered rock samples were extracted using a Dionex ASE 350 accelerated solvent extractor. A dichloromethane solvent was used at confined conditions of 75 °C and 110 bar (full details of this procedure are given in Gross et al., 2015). The saturated compounds were further separated into normal alkanes and branched–cyclic alkanes for compound-specific isotopic analyses using an activated molecular sieve (Merck, 500 pm pore space), cyclohexane, and a cyclohexane–n-pentane (12:88) solution.

Saturated and aromatic hydrocarbon fractions were analysed using a gas chromatograph equipped with a 30 m DB-5MS fused silica capillary column (i.d. 0.25 mm; 0.25 µm film thickness) and coupled to a ThermoFisher ISQ mass spectrometer. The measuring process followed is described in Gross et al. (2015).

Stable carbon isotope measurements of *n*-alkanes and acyclic isoprenoids were performed on selected samples using a Trace GC instrument attached to a ThermoFisher DELTA-V isotope ratio mass spectrometer via a combustion interface (GC isolink, ThermoFisher).

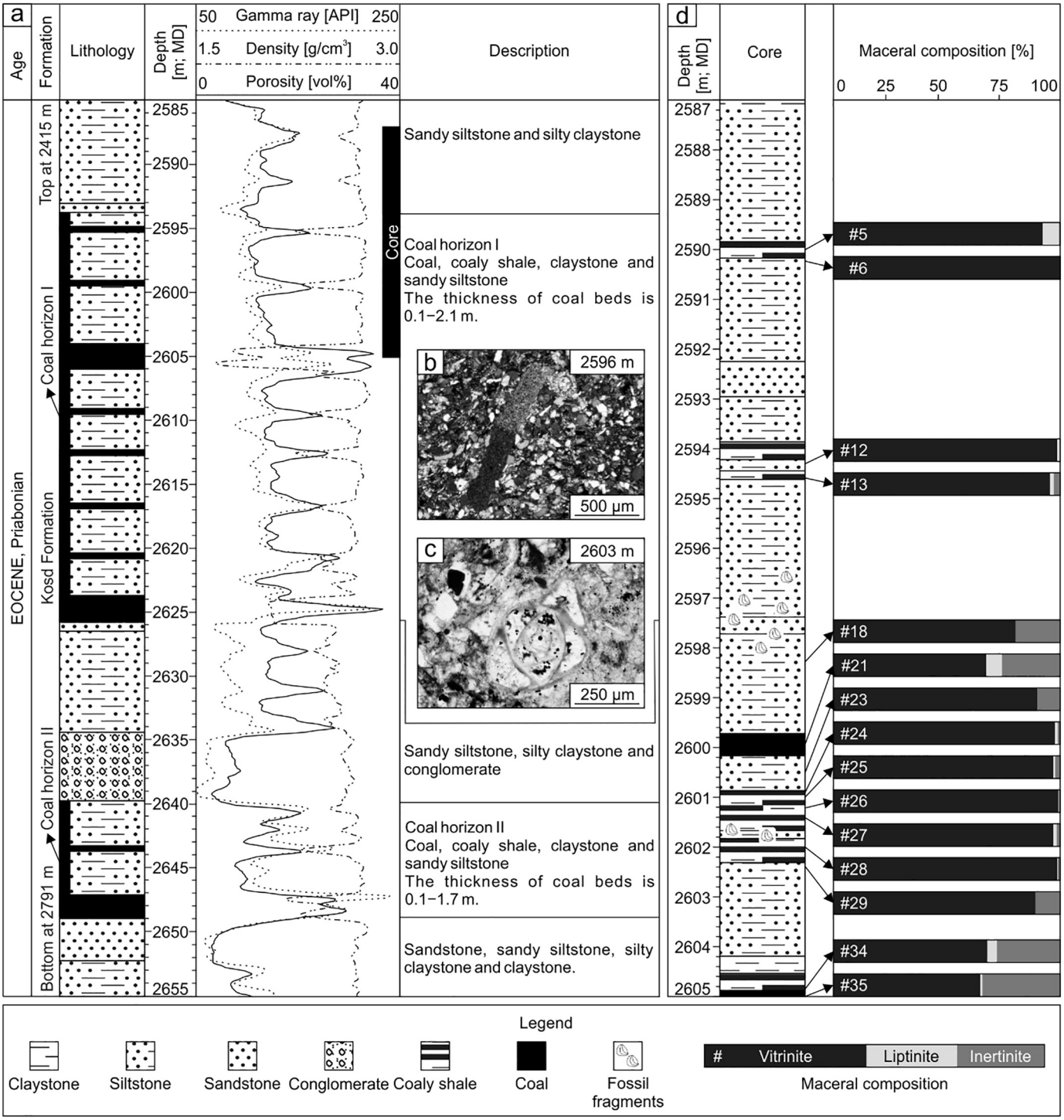

Fig. 3. Simplified lithostratigraphy of the investigated section at the W–1 well. a) Lithologies are assigned based on well logs and drill cuttings. Drill core was recovered from 2587 m to 2605 m. b) Preserved fossils in the siltstone, including echinoid fragment (crossed Nicols) and c) miliolid foraminifer (plane polarized light). d) Location of organic matter rich samples in the higher resolution stratigraphy sequence selected for organic petrology and their maceral composition. Sample depth is given as measured depth (MD).

CO_2 was injected at the beginning and the end of each analysis in order to perform instrumental calibration. The GC column and temperature program used were the same as above. Stable isotope ratios are reported in delta notation ($\delta^{13}C$; Coplen, 2011) relative to the Vienna Pee Dee Belemnite (V-PDB) standard ($\delta^{13}C = [(\delta^{13}C/\delta^{12}C)_{sample}/(\delta^{13}C/\delta^{12}C)_{standard} - 1]$). Delta notation is expressed in parts per thousand or per mil (‰). The analytical error was better than 0.2‰.

4. Results

4.1. Lithology

Based on drill cuttings and well logs (gamma ray, density, porosity) the Kosd Formation is 376 m thick and includes two coal horizons at depths between 2594 and 2649 m (Fig. 3a). The lower and upper coal horizons are about 9 m and 36 m thick, respectively. The sediments

between the coal horizons consist of grey sandstone, sandy siltstone, silty claystone, and conglomerate. Non-coal layers within the coal horizons comprise grey, sandy-, argillaceous-, calcareous- and coaly siltstones. Individual coal beds are 0.1 to 2.1 m thick and include coal and coaly shale, and intercalations of siltstone and claystone (Fig. 3a).

The studied drill core (2587–2605 m depth) represents the upper portion of the coal horizon I (Fig. 3a). Its base is located in the upper part of a 2 m-thick coal bed at a depth of 2605 m. The core includes coal layers, which are black, consolidated and hard. Two different lithotypes can be distinguished: (i) a generally bright, finely banded clarain coal, which is brittle, exhibits uneven fracture and occurs as 5 to 50 cm thick layers; and (ii) a stratified coaly shale, including intercalations of thin (< 1 cm) siltstone and claystone layers, in which the thickness varies from 5 to 40 cm. The interseam sediments are dominated by sandy siltstone, which is variably calcareous and argillaceous. Original sedimentary structures are not visible due to bioturbation, however, slumps are recognizable. Two distinct intervals with shell fragments are observed (2596.5–2598.0 m; 2601.5–2602.0 m). Microscopic investigation revealed that the siltstone is rich in fossils, including mollusc, brachiopod, echinoid fragments and miliolid foraminifers (Figs. 3b, c).

4.2. Bulk geochemical parameters

The TOC contents of coal and coaly shale range between 45.7 and 78.4 wt% (avg. 60.4 wt%) and between 12.7 and 29.5 wt% (avg. 22.3 wt%), respectively, whereas the TOC contents of the interseam lithologies vary between 0.4 and 7.2 wt% (avg. 1.3 wt%). Generally, the TOC contents of samples are greater than 2.9 wt% from 2599.9 m to 2602.0 m (#21 to #28), including coal beds and interseam sediments (Table 1). The ash yield of coals varies between 5.8 and 77.9 wt% (Table 1). The maximum calcite equivalent percentage in coals and intercalating sediments is 6.8 and 36.1 wt% (avg. 4.0 and 10.0 wt%), respectively (Table 1).

The sulphur content of coaly layers ranges between 3.4 and 8.8 wt% (avg. 4.9 wt%). In the non-coaly intervals, sulphur contents vary between 1.4 and 4.8 wt% (avg. 2.8 wt%). In most cases, below the depth of 2599 m (#20), the sulphur contents are greater than 2.8 wt%, except sample #35. The TOC/TS ratio varies between 3.6 and 23.0 (avg. 9.2) in coaly lithotypes, whereas its value in interseam sediments ranges from 0.2 to 4.6 (avg. 0.5; Table 1).

Tmax values range from 431 to 448 °C (Table 1). The HI ranges from 36 to 291 mg HC/g TOC (Table 1). In Tmax vs. HI plots (Figs. 4a, b), samples can be subdivided into two populations, reflecting those with less or more than 150 mg HC/g TOC. The HI of coaly lithotypes varies from 229 to 291 mg HC/g TOC (avg. 252 mg HC/g TOC). The HI in the interseam sediments is from 36 to 289 mg HC/g TOC (avg. 87 mg HC/g TOC), however, higher readings (> 150 mg HC/g TOC) were recorded at samples #6, #25 and #27, which are adjacent to coals (Table 1). BI and QI were calculated for coals and coaly shales, and vary from 30 to 37 mg HC/g TOC and from 259 to 323 mg HC/g TOC, respectively (Figs. 4c, d; Table 1). An important observation noted during Rock-Eval pyrolysis is that coaly samples undergo stronger swelling, i.e. their volume increases significantly during heating.

The amount of extractable organic matter (EOM) varies between 31 and 212 mg/g TOC and yields of EOM are usually higher in intercalating sediments (Table 3). EOM is dominated by polar compounds (34–50 wt%), except in samples #20 and #29, where the saturated compounds are prevalent (38 and 43 wt%, respectively). The saturated and aromatic hydrocarbon contents ranging from 5 to 43 wt% and 14 to 28 wt%, respectively. The amount of asphaltene is between 9 and 31 wt % (Table 3). Aside from the general dominance of polar compounds, coaly lithotypes are found to be characterized by similar average percentages of aromatic hydrocarbons and asphaltenes (avg. 24 and 25 wt %, respectively), and the quantity of saturated hydrocarbons is low (avg. 5 wt%). In contrast, interseam lithologies are characterized by similar amounts of saturated and aromatic hydrocarbons (avg. 24 and 22 wt%, respectively) and a lower amount of asphaltenes (avg. 13 wt%; Table 3).

4.3. Maceral composition and vitrinite reflectance

Maceral analyses were performed on 15 samples, including coal, coaly shale, and claystone/siltstone (Table 2). Vitrinite group macerals predominate in all samples (Figs. 3d, 5; Table 2). In coals, vitrinite macerals account for between 67 and 99 vol%. Collotelinite (37–46 vol %), collodetrinite (7–48 vol%) and gelinite (10–21 vol%) are the most abundant vitrinite macerals present. Collotelinite and collodetrinite exhibit an orange-brown fluorescent colour under UV light irradiation (Fig. 5). Inertinite macerals are typically in the range of 1 to 3 vol% but reach significantly higher values in banded coal samples (26 and 28 vol %, in #21 and #34, respectively). In banded coal samples, funginite and inertodetrinite are present in addition to fusinite. The percentages of liptinite macerals reach 8 vol% and sporinite and alginite are present in substantial amounts (max. 4 vol%) in some samples.

In claystone/siltstone samples, vitrinite maceral contents vary from 65 to 100 vol%. Inertinite macerals are abundant in the lowermost sample (#35: 34 vol%; Fig. 3d; Table 2). Liptinite macerals, mainly sporinite, are generally rare and do not exceed 2 vol% (Fig. 3d; Table 2). Framboidal pyrite occurs in substantial quantity throughout all samples, however, the highest contents are observed in the claystone/siltstone samples (Table 2).

Vegetation- (VI) and groundwater influence indices (GWI_{AC}) were calculated for coaly sediments based on Calder et al. (1991) and Stock et al. (2016; Fig. 6; Table 2). VI ranges from 0.7 to 4.8 and GWI_{AC} varies between 2.9 and 39.2 (Table 2).

Mean random vitrinite reflectance was found to range from 0.67 to 0.78 (Table 2).

4.4. Molecular composition of hydrocarbons

4.4.1. Straight chain alkanes and isoprenoids

The concentration of *n*-alkanes (Tables 3, 4) varies considerably across the investigated section. The compositions of identified *n*-alkanes vary within the range of *n*-C_{13} to *n*-C_{37}. Patterns of *n*-alkane distribution are characterized by a relatively uniform proportion of mid-chain *n*-alkanes (*n*-C_{21-25}; 27–38% of the total *n*-alkanes; Fig. 7; Table 4). Coaly lithologies (#21, #24, #26 and #28) and their adjacent sediments (#22 and #27) are dominated by short-chain *n*-alkanes (*n*-C_{15-19}; 30–46%; Fig. 8). In contrast, interseam lithologies are generally dominated by long-chain *n*-alkanes (*n*-C_{27-31}; 24–31%; Fig. 8). Furthermore, n-alkane envelopes exhibit a bimodal distribution pattern. The carbon preference index (CPI; Bray and Evans, 1961) is close to one (0.93–1.04, Table 4).

The acyclic isoprenoids, including *i*-C_{13}, farnesane, *i*-C_{16}, norpristane, pristane (Pr) and phytane (Ph), are present in great abundance in all samples (Table 3). The ratios of Pr/Ph range from 3.0 to 4.2 (Table 4).

The stable carbon isotopic composition ($\delta^{13}C$) of *n*-alkanes, Pr and Ph is similar for all studied samples (Fig. 9). With increasing chain length, $\delta^{13}C$ values of the *n*-C_{15-19} and *n*-C_{21-25} alkanes of selected samples show a decline of about 1‰, respectively. In contrast, long-chain alkanes (*n*-C_{27+}) show a reversed trend and increasing $\delta^{13}C$ with carbon number. Pr and Ph exhibit similar isotopic compositions, but Ph is observed to be slightly depleted in ^{13}C in comparison to Pr (Fig. 9).

4.4.2. Steroids

The concentration of steranes is very low in all samples (Table 3), however, in the saturated hydrocarbon fraction, 5α,14α,17α(H) steranes dominate over 5β,14α,17α(H) isomers, and are present in the C_{27}–C_{29} range. Normalized values of steranes were plotted on a ternary diagram of C_{27}, C_{28} and C_{29} regular steranes (Huang and Meinshein, 1979), showing the relative distribution of steranes indicating organic matter depositional facies (Fig. 10). C_{29} homologues are found to

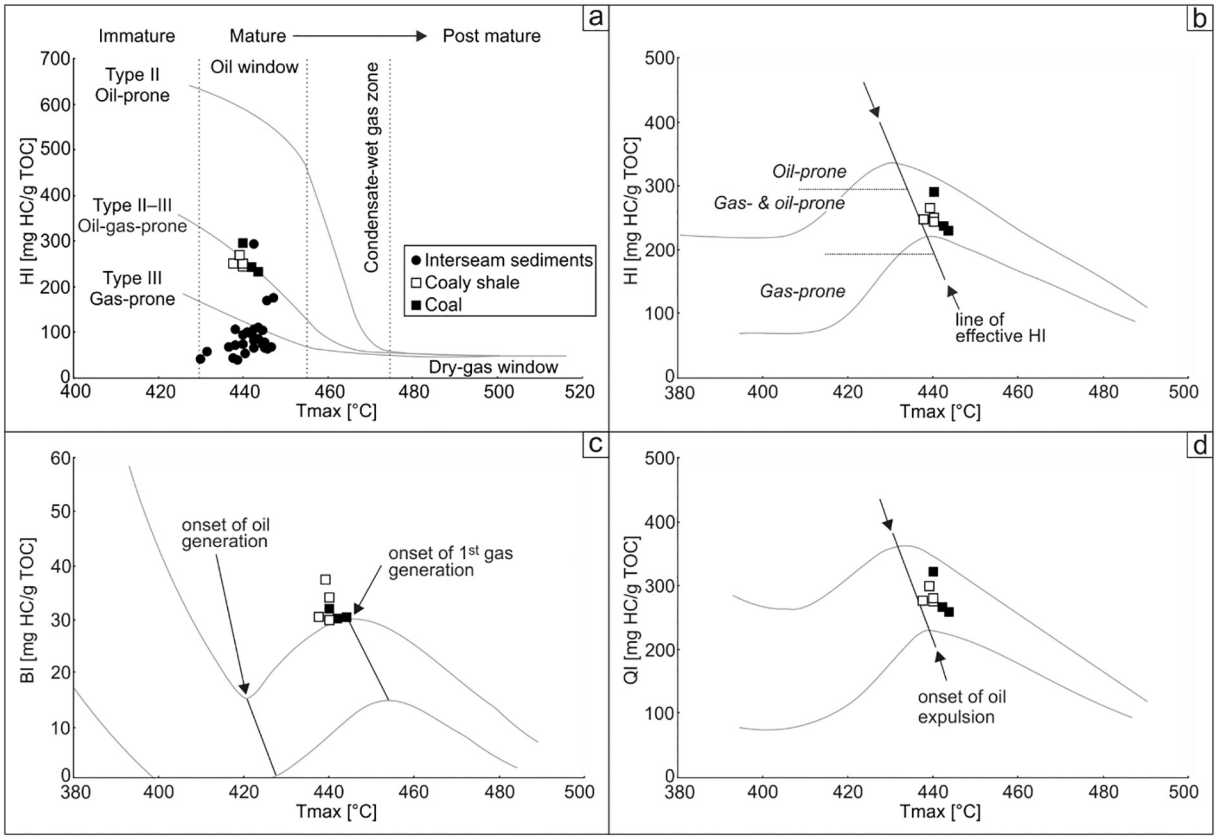

Fig. 4. Petroleum potential assessment. a) Plot of Tmax vs. HI, showing the maturity and type of kerogen present in the investigated samples (after Espitalié et al., 1984). b) Plot of Tmax vs. HI, highlighting the increase in HI prior to the onset of oil expulsion (after Sykes and Snowdon, 2002). c) Rank threshold for oil- and gas generation indicated by BI (after Sykes and Snowdon, 2002). d) Rank threshold for oil expulsion determined by QI (after Sykes and Snowdon, 2002).

Table 2
Mineral matter-free (mmf) maceral-, mineral composition, petrographic indices and random vitrinite reflectance of the investigated samples.

ID	Ct	Vd	Cd	Cg	G	Σ VIT	S	A	Σ LIP	F	Sf	Fg	Ma	Mi	Id	Σ IN	Pyr	DM	VI	GWI_{AC}	%Rr ± SD
#	[vol%, mmf]																[vol%]				
5	44.0	4.0	33.1	–	9.8	90.9	3.5	3.9	7.4	0.5	1.2	–	–	–	–	1.8	17.4	44.7	1.1	29.8	0.72 ± 0.03
6	–	–	–	–	–	100.0	–	–	–	–	–	–	–	–	–	–	25.0	71.0	–	–	0.73 ± 0.05
12	–	–	–	–	–	98.7	–	–	1.3	–	–	–	–	–	–	–	13.2	73.8	–	–	0.68 ± 0.05
13	45.9	–	32.2	–	17.4	95.5	1.1	0.5	1.6	1.0	1.8	–	–	–	–	2.8	8.5	27.6	1.4	39.2	0.73 ± 0.04
18	–	–	–	–	–	80.4	–	–	–	–	–	–	–	–	–	19.6	17.3	79.3	–	–	0.74 ± 0.06
21	59.1	–	7.4	0.6	0.2	67.4	5.7	1.3	6.9	9.1	12.7	0.3	–	1.1	2.5	25.7	0.1	0.8	4.8	2.9	0.76 ± 0.04
23	–	–	–	–	–	90.0	–	–	–	–	–	–	–	–	–	10.0	13.3	78.7	–	–	0.78 ± 0.06
24	36.9	–	40.2	–	20.6	97.7	1.2	–	1.2	0.4	0.6	–	–	–	–	1.0	8.8	24.0	0.9	16.3	0.71 ± 0.02
25	–	–	–	–	–	97.0	–	–	0.8	–	–	–	–	–	–	2.3	15.8	76.1	–	–	0.78 ± 0.04
26	32.8	0.6	47.7	–	17.0	98.1	0.5	–	0.5	0.6	0.8	–	–	–	–	1.4	8.2	28.9	0.7	31.2	0.68 ± 0.02
27	–	–	–	–	–	97.0	–	–	1.5	–	–	–	–	–	–	1.5	14.5	73.2	–	–	0.75 ± 0.03
28	38.2	–	40.1	–	20.3	98.7	0.3	–	0.3	0.6	0.4	–	–	–	–	1.0	6.1	50.2	1.0	33.4	0.67 ± 0.04
29	–	–	–	–	–	90.9	–	–	–	–	–	–	–	–	–	9.1	4.4	92.0	–	–	0.73 ± 0.06
34	48.5	0.4	9.8	2.8	6.4	67.9	4.1	–	4.1	16.7	4.8	0.1	1.4	1.0	3.8	27.9	8.0	44.7	4.1	15.4	0.75 ± 0.03
35	–	–	–	–	–	64.8	–	–	0.9	–	–	–	–	–	–	34.3	14.8	78.2	–	–	0.74 ± 0.04

Macerals that were not counted and are in very low percentages (< < 0.1 vol%) are not included in the table, however, resinite, liptodetrinite and cutinite occur in the samples. Ct – collotelinite, Vd – vitrodetrinite, Cd – collodetrinite, Cg – corpogelinite, G – gelinite, Σ VIT – total vitrinite, S – sporinite, A – alginite, Σ LIP – total liptinite, F – fusinite, Sf – semifusinite, Fg – funginite, Ma – macrinite, Mi – micrinite, Id – inertodetrinite, Σ IN – total inertinite, Pyr – pyrite, DM – detrital minerals, VI – vegetation index, GWI_{AC} – groundwater index, %Rr ± SD – mean random vitrinite reflectance ± standard deviation. VI = (telovitrinite + fusinite + semifusinite + cutinite + sporinite + suberinite + resinite) / (detrovitrinite + inertodetrinite + alginite + liptodetrinite + exsudatinite + chlorophyllinite + bituminite; Calder et al., 1991), GWI_{AC} = (gelovitrinite + (ash yield / 2)) / (telovitrinite + vitrodetrinite); Stock et al., 2016).

prevail in the samples, followed by C_{28} and C_{27} steranes. In organic matter-rich samples, C_{29} steranes predominate in the distributions (Fig. 10; Table 3). The corresponding diasteranes are found in even lower abundance (Table 3), and exhibit similar carbon number distributions as the regular steranes. In the aromatic hydrocarbon fractions, monoaromatic (C_{29}) stigmastanes and triaromatic (C_{28}) stigmastanes were identified at very low concentrations.

The stereoisomer ratios of S/(S + R) of ααα C_{29} steranes and ββ/(ββ + αα) of C_{29} steranes were assessed as a thermal maturity parameter. Ratios of the 20S/(20S + 20R) isomers of the 5α,14α,17α(H)–C_{29} steranes range between 0.40 and 0.53. Moreover, ratios of αββ/(αββ + ααα) isomers of C_{29} steranes range from 0.65 to

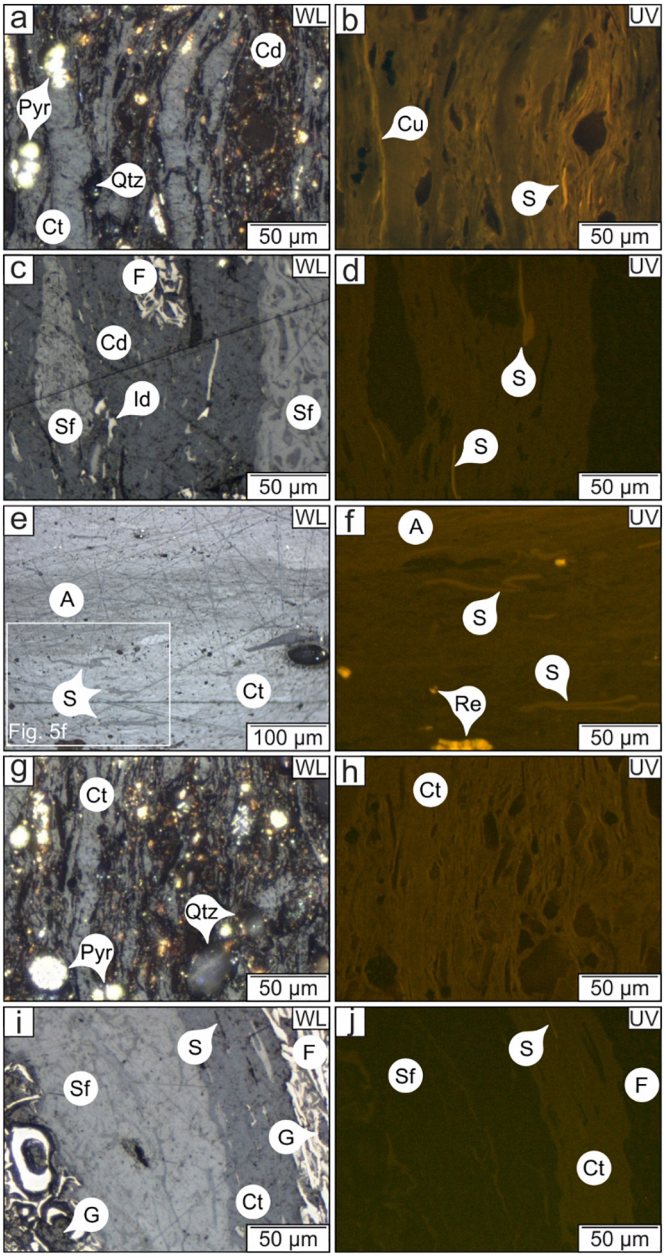

Fig. 5. Photomicrographs of coal samples studied. Images were taken under reflected white light (WL) and ultraviolet light (UV) using oil immersion objective. Samples are #5 (a, b), #21 (c, d, e, f), #26 (g, h) and #34 (i, j). A – alginite, Cd – collodetrinite, Ct – collotelinite, Cu – cutinite, F – fusinite, G – gelinite, Id – inertodetrinite, Pyr – pyrite, Qtz – quartz, Re – resinite, S – sporinite and Sf – semifusinite.

0.69 (Table 4).

4.4.3. Hopanoids

Hopanoids are important constituents of the non-aromatic cyclic triterpenoids (Table 3). The measured hopanoid patterns are characterized by the occurrence of 17α,21β(H)– and 17β,21β(H)–type hopanes from C_{27} to C_{35} with C_{28} hopanes being absent. The predominant hopanoids in most samples are 17α,21β–C_{30} and 17β,21α–C_{29} hopane. The 17α,21β(H)–type homohopanes show a dominant pattern of exponential decrease in peak height with increasing carbon number. In most samples, a series of C_{32}– to C_{35}–benzohopanes was identified in the aromatic hydrocarbon fractions. In all investigated samples, the ratios of steroids to hopanoids are between 0.06 and 0.15 (Table 4).

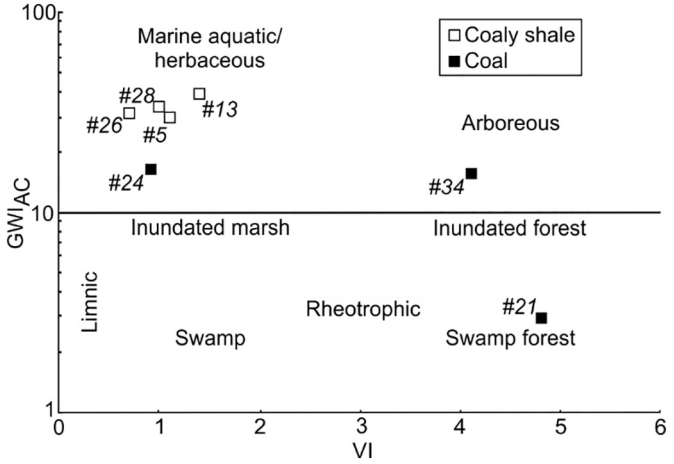

Fig. 6. Chart of vegetation- (VI) and groundwater influence index (GWI_{AC}; after Calder et al., 1991).

The stereoisomer ratio of 22S/(22S + 22R) isomers of 17α,21β(H)–C_{32} hopanes, a thermal maturity parameter, ranges from 0.55 to 0.63 (Table 4).

4.4.4. Sesquiterpenoids, diterpenoids, non-hopanoid triterpenoids

Bicyclic sesquiterpenoids are characterized by the occurrence of 8β(H)–homodrimane, 8β(H)–drimane, and 4β(H)–eudesmane. Furthermore, rearranged drimenes and pentamethyl–trans–decalins are also present in the studied samples. Decalins were identified as 2,2,4a,7,8–pentamethyl–trans–decalin and 1,2,2,5,5–pentamethyl–-trans–decalin according to Nytoft et al. (2009). Diterpenoids consist of bicyclic- (8β(H)–labdane), tricyclic- (pimarane, isopimarane and abietane) and tetracyclic diterpanes (16β(H)–phyllocladane). The tetra- and pentacyclic triterpenoids occur in the analysed samples and the following oleanane, ursane and lupane types were identified in non-aromatic hydrocarbon fractions: des–A–olean–12–ene, des–A–urs–12–ene, 10β(H)–des–A–oleanane, 10β(H)–des–A–lupane, 10β(H)–des–A–ursane, lupane, urs–12–ene, and 18β(H)–oleanane, with a substantial amount of 18α(H)–oleanane.

Aromatic sesquiterpenes are represented by cadalene, calamenene and 5,6,7,8–tetrahydrocadalene. Abietane-type aromatic diterpenoids are present and consist of 1,2,3,4–tetrahydroretene, norsimonellite, simonellite, and retene. The following aromatic tetra- and pentacyclic triterpenoids are identified in the aromatic hydrocarbon fractions: tetramethyl–octahydro–chrysenes, trimethyl–tetrahydro–chrysenes, and tri- and tetra aromatic pentacyclic triterpenoids of the oleanane- and ursane-types (tetramethyl–octahydro–picenes, trimethyl–tetrahydro–picenes).

4.4.5. Polycyclic aromatic hydrocarbons

The total ion chromatograms of aromatic hydrocarbon fractions are dominated by naphthalenes and phenanthrenes (Table 3). Naphthalene (N) occurs at low concentrations, however, its alkylated counterparts, methyl- (MN), dimethyl- (DMN) and trimethylnaphthalenes (TMN), are present at a higher amount. The methylnaphthalenes (2– and 1–MN) are present in equal quantities, whereas 1,6–DMN and 1,2,5– and 1,2,7–TMN predominate the dimethyl- and trimethylnaphthalenes, respectively.

Phenanthrene (P), alkylated phenanthrenes (methyl- (MP), dimethyl- (DMP) and trimethylphenanthrenes (TMP)) occur in considerable concentrations in the investigated samples. The 9–, 1– and 2–MP characterize the methylphenanthrenes. The methylphenantrene index (MPI 1; Radke et al., 1982) varies between 0.52 and 0.59 and calculated vitrinite reflectance values ($\%R_{c(MPI\ 1)}$; Radke and Welte, 1983) vary between 0.71 and 0.75%Rc (Table 4). The pattern of

Table 3
Rock extracts, percentage of extract fractions and concentrations of hydrocarbon species of investigated samples in the Kosd Formation.

ID	a	b	c	d	e	f	g	h	i	j	k	l	m	n	o	p	q	r	s	t	u	v	w
#	[mg/g TOC]	[wt%]				[µg/g TOC]																	
20	164	38	19	35	9	14973	2082	44	10	221	74	241	17	112	218	300	1	1336	270	1682	244	1050	216
21	31	5	26	50	19	235	78	5	1	56	21	98	2	25	21	113	12	1245	112	515	95	300	87
22	84	10	28	48	13	2018	524	11	2	59	49	321	5	100	54	373	1	3300	319	1809	321	1228	285
23	146	26	21	40	13	11588	2605	55	12	233	257	379	21	88	586	256	56	2348	220	1198	231	994	209
24	57	5	23	46	25	410	158	14	1	60	41	151	8	38	115	131	8	1277	129	630	129	452	102
25	95	13	27	42	18	2497	794	20	4	83	123	297	12	66	239	216	10	2087	190	1007	201	811	169
26	60	6	24	46	24	733	223	14	2	28	35	211	4	38	154	166	3	1451	159	703	161	475	139
27	83	12	24	47	17	2527	571	14	3	96	85	247	8	53	261	276	4	2125	236	1118	235	842	220
28	62	6	21	42	31	639	159	9	1	77	35	142	4	27	108	172	2	1334	159	691	149	497	131
29	212	43	14	34	9	28999	3485	76	21	351	151	254	21	48	908	173	1	843	262	1399	198	835	212

a – extracted organic matter, b – saturated hydrocarbons, c – aromatic hydrocarbons, d – polar compounds, e – asphaltenes, f – *n*-alkanes, g – isoprenoids, h – steranes, i – diasteranes, j – hopanes, k – sesquiterpenoids, l – aromatic sesquiterpenoids, m – diterpenoids, n – aromatic diterpenoids, o – triterpenoids, p – aromatic triterpenoids, q – naphthalenes, r – alkylated naphthalenes, s – phenanthrenes, t – alkylated phenanthrenes, u – dibenzothiophenes, v – alkylated dibenzothiophenes, w – benzonaphthothiophenes.

dimethylphenanthrenes is predominated by 1,7–DMP, and the co-eluting 1,3,7–, 1,3,9– and 2,7,10–TMP dominate the trimethylphenanthrenes.

Beside the naphthalenes and phenanthrenes, polycyclic aromatic hydrocarbons identified include chrysene, alkylated chrysenes, and perylene.

4.4.6. Sulphur-aromatic compounds

The sulphur-containing aromatic compounds identified include dibenzothiophenes and benzonaphthothiophenes, both of which occur in considerable quantities in the investigated samples (Table 3). Dibenzothiophenes are represented by dibenzothiophene (DBT), methyl- (MDBT), dimethyl- (DMDBT) and trimethyldibenzothiophenes (TMDBT). Methyldibenzothiophenes are characterized by 4–MDBT, co-eluting 3– + 2–MDBT and 1–MDBT, in descending order of concentration. The benzonaphthothiophenes are dominated by benzo[*b*]naphtho[2,1]thiophene, whereas benzo[*b*]naphtho[1,2]thiophene and benzo[*b*]naphtho[2,3]thiophene occur in lower quantities.

The DBT/P ratios (Hughes et al., 1995) range between 0.74 and 1.04 (Fig. 11; Table 4).

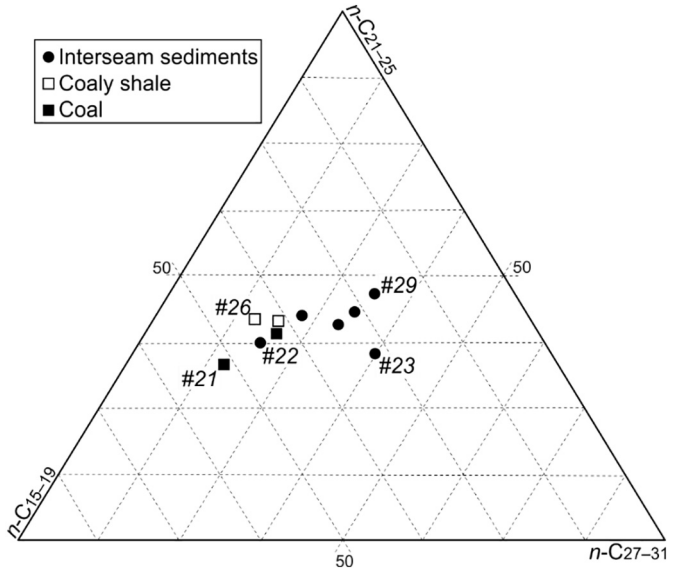

Fig. 7. Normalized distribution of short- (*n*-$C_{15–19}$), mid- (*n*-$C_{21–25}$) and long-chain (*n*-$C_{27–31}$) *n*-alkanes in the studied samples.

5. Discussion

5.1. Thermal maturity

Vitrinite reflectance (0.67–0.78%Rr; Table 2) and Tmax values (431–448 °C; Table 1) indicate that the coals of the Kosd Formation reached high volatile bituminous rank (Taylor et al., 1998) and that the organic matter is mature, but did not yet reach peak oil window maturity (0.8%Rr, e.g. Peters and Cassa, 1994). Nevertheless, values of Rr and Tmax vary slightly and point to lower values in coaly lithotypes. The content of liptinite group macerals is limited, however, organic

Table 4
Concentration ratios of compounds in hydrocarbon fractions of samples from the Kosd Formation.

ID	a	b	c	d	e	f	g	h	i	j	k	l	m	n	o
#		[%]					[%]						[%]		
20	22	35	25	1.00	3.30	30	24	46	0.13	0.42	0.65	0.55	0.75	0.89	0.20
21	46	27	12	1.04	4.10	14	23	63	0.06	0.50	0.67	0.57	0.71	0.83	0.17
22	39	31	15	0.97	4.22	20	23	57	0.11	0.53	0.68	0.56	0.73	0.99	0.20
23	18	29	31	0.97	3.52	26	30	44	0.10	0.43	0.66	0.59	0.74	1.03	0.11
24	35	32	17	0.96	3.76	17	17	66	0.11	0.45	0.67	0.59	0.73	0.98	0.16
25	24	33	24	0.97	3.96	26	28	45	0.10	0.44	0.67	0.57	0.72	1.04	0.15
26	34	34	16	0.93	3.63	21	27	52	0.15	0.42	0.66	0.63	0.72	1.00	0.12
27	30	35	19	1.00	3.57	25	28	46	0.06	0.46	0.66	0.59	0.73	0.98	0.10
28	37	34	13	0.96	3.30	18	20	62	0.06	0.49	0.69	0.57	0.72	0.92	0.10
29	17	38	26	1.03	3.01	38	26	36	0.09	0.40	0.66	0.57	0.73	0.74	0.06

a – *n*-$C_{15–19}$/*n*-$C_{15–35}$, b – *n*-$C_{21–25}$/*n*-$C_{15–35}$, c – *n*-$C_{27–31}$/*n*-$C_{15–35}$, d – CPI (Bray and Evans, 1961), e – Pr/Ph, f – C_{27} steranes/Σ regular steranes, g – C_{28} steranes/Σ regular steranes, h – C_{29} steranes/Σ regular steranes, i – steranes/hopanes, j – 20S/(20S + 20R) ααα C_{29} steranes, k – αββ/(αββ + ααα) C_{29} steranes, l – 22S/(22S + 22R) C_{32} hopane, m – $R_{c(MPI\ 1)}$ (Radke and Welte, 1983), n – DBT/P (Hughes et al., 1995), o – Di- / (Di- + Triterpenoids; Bechtel et al., 2003).

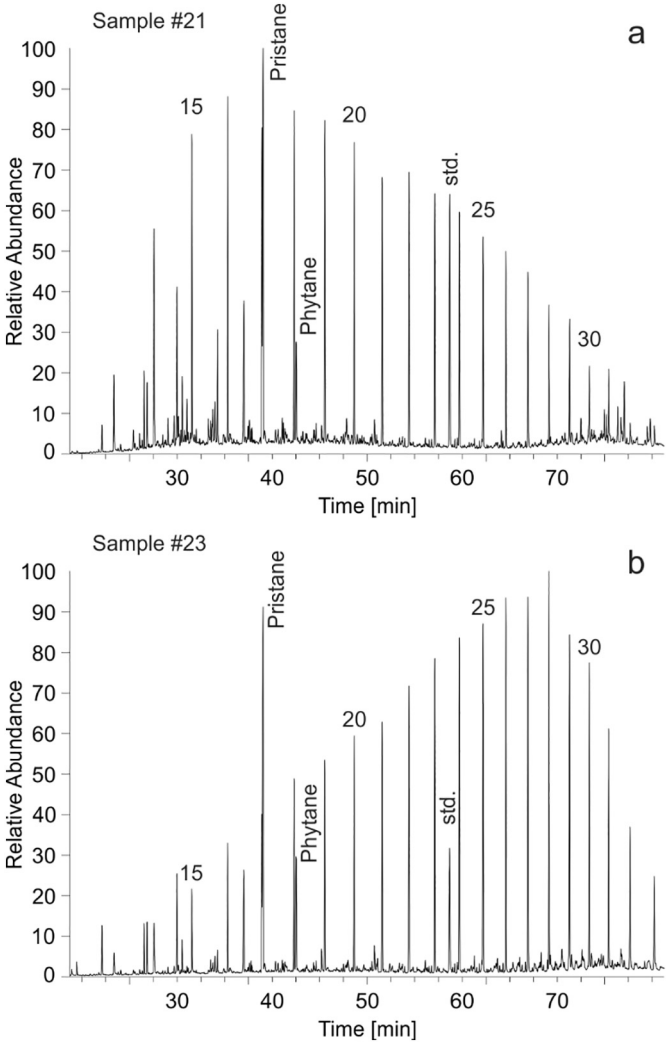

Fig. 8. Gas chromatograms (total ion current) of saturated hydrocarbon fraction of (a) coal, sample #21 and (b) claystone, sample #23. *n*-Alkanes are labelled according to the carbon number. std. – standard (deuterated n-tetracosane).

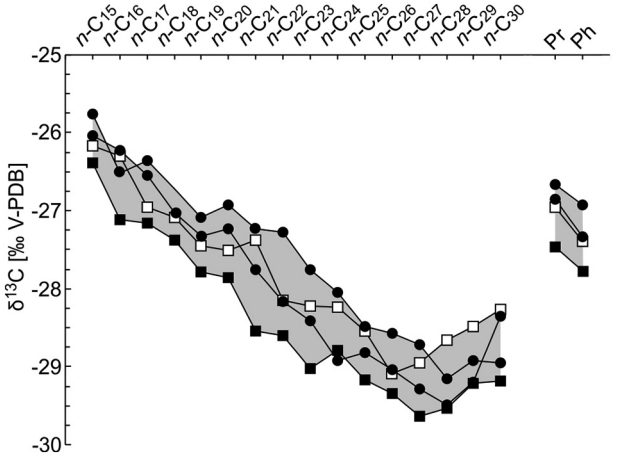

Fig. 9. Carbon isotopic composition of *n*-alkanes, pristane and phytane in coal (#24), coaly shale (#26) and interseam sediments (#25, #27).

matter is dominated by fluorescent vitrinite (Fig. 5; Table 2). The orange-brown fluorescence colour of the vitrinite and the strong swelling during pyrolysis both suggest the predominance of hydrogen-rich

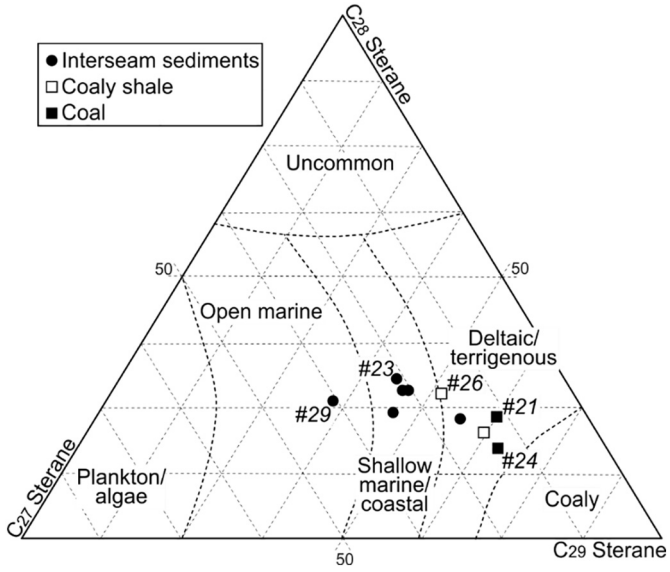

Fig. 10. Ternary plot of regular steranes showing the normalized abundance of C_{27}, C_{28} and C_{29} sterane isomers and their depositional facies (after Huang and Meinshein, 1979).

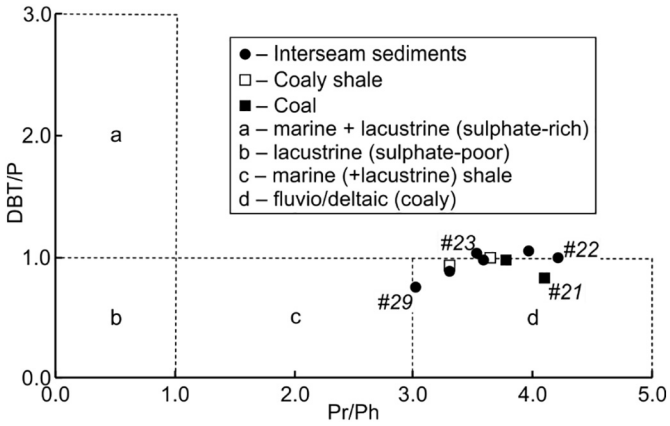

Fig. 11. Cross-plot of pristane/phytane (Pr/Ph) vs. dibenzothiophene/phenanthrene (DBT/P) ratios (after Hughes et al., 1995).

vitrinite (Wilkins and George, 2002). Hence, the vitrinite reflectance of coaly lithotypes may be suppressed due to the diagenetic enrichment in hydrogen and sulphur (e.g. Peters et al., 2018 cum *lit.*). Considering the relatively low content of liptinite macerals and extractable organic matter, suppression due to sorption of generated bitumen (Carr, 2000; Taylor et al., 1998; Wilkins and George, 2002) seems less likely.

Hopane (22S/22S + 22R C_{32}) and sterane (20S/(20S + 20R) ααα C_{29}) isomerisation ratios range from 0.55 to 0.63 and from 0.40 to 0.53, respectively (Table 4). Although this indicates that C_{32} hopane isomerisation ratios reached their equilibrium value, sterane isomerisation ratios of C_{29} suggest that steranes did not. This denotes maturities corresponding to the oil window (0.6–0.8%Rr; Mackenzie et al., 1980; Mackenzie and Maxwell, 1981; Seifert and Moldowan, 1986; Peters et al., 2005). This maturity assessment is supported by ratios of ββ/(ββ + αα) isomers of the 5α,14α,17α (H)–C_{29} steranes (0.65–0.69; Table 4), which are close to their equilibrium value of 0.7 (Seifert and Moldowan, 1986). CPI values close to one (0.93–1.04) further confirm this maturity assessment.

The methylphenanthrene index (MPI) is a well-established parameter for classifying maturity (Radke et al., 1982) and can be used to calculate vitrinite reflectance values (Radke and Welte, 1983). The calculated vitrinite reflectance values are between 0.71 and 0.75%Rc

(Table 4), which fits well with the measured values.

5.2. Source of organic matter

The Kosd coal is generally dominated by vitrinite and inertinite subgroup macerals (Table 2), which are derived from woody tissues of herbaceous and arborescent plants (ICCP, 1998). Petrography-based facies indicators have been determined for the coaly lithotypes. The vegetation index (VI; Table 2) contrasts macerals of forest affinity with those of herbaceous and marginal aquatic affinity (Calder et al., 1991). All studied samples of Kosd coal, except #21 and #34, are characterized by VI values below 3 (Fig. 6; Table 2), indicating a predominance of herbaceous peat-forming flora.

Long-chain lipids are typically attributed to higher terrestrial plants (Eglinton and Hamilton, 1967), whereas mid-chain *n*-alkanes are reported in aquatic macrophytes and *Sphagnum* (Bingham et al., 2010; Dehmer, 1995; Ficken et al., 2000; Nott et al., 2000), and short-chain *n*-alkanes are identified predominantly in algae and other microorganisms (Cranwell, 1977; Cranwell et al., 1987). Hence, it is surprising that the studied coaly samples (TOC > 20 wt%) are characterized by significantly higher amounts of short-chain *n*-alkanes than long-chain *n*-alkanes (Table 4). For example, the clean coal #21 (TOC 78.4 wt%; ash yield: 5.2 wt%) contains the highest relative percentage of short-chain *n*-alkanes (max. 46%) and the lowest relative percentage of long-chain *n*-alkanes (min. 12%; Table 4). A shift towards shorter *n*-alkanes may be caused by advanced maturity (e.g. Radke et al., 1980), but this effect alone cannot explain the pattern observed since some low-TOC samples also contain high percentages of long-chain *n*-alkanes (e.g. #23; 31%). The high amounts of short-chain *n*-alkanes in coal samples are related to the strong fluorescence of vitrinite macerals, high S1 and BI values (Table 1; Fig. 4c) and may be caused by either migration (Littke et al., 1990) or bacterial activity. Whereas relative amounts of long- and short-chain *n*-alkanes vary significantly, mid-chain *n*-alkanes are found at high, relatively constant proportions (27–34%).

δ^{13}C-values of *n*-alkanes in the selected samples (Fig. 9) are consistent with previous studies performed on coal samples (e.g. Gross et al., 2015; Schoell et al., 1994; Simoneit et al., 1995; Schwarzbauer et al., 2013; Tuo et al., 2003). Variations of carbon isotopic compositions of individual compounds are within 1‰, indicating a positive correlation between sample sets (Sofer, 1984). δ^{13}C-values also show a decreasing trend, becoming more depleted in ^{13}C with increasing chain length in all samples (Fig. 9), a phenomenon often observed in coals (e.g. Doković et al., 2018; Schoell et al., 1994; Schwarzbauer et al., 2013; Tuo et al., 2003). The long-chain *n*-alkane compounds, however, show an opposite tendency, getting more enriched in ^{13}C with increasing chain length (Fig. 9). Both long-chain *n*-alkane production and the biosynthetic fractionation of carbon isotopes vary among plant types (Diefendorf et al., 2011; Lockheart et al., 1997) and studies have pointed to ^{13}C enrichment with chain length in recent terrestrial plants (e.g. Collister et al., 1994; Diefendorf et al., 2011; Diefendorf et al., 2015; Lockheart et al., 1997; Mead et al., 2005). Nevertheless, the effect of thermal maturation on the carbon isotopic composition of organic matter has already been considered by several authors (e.g. Bjorøy et al., 1992; Rooney et al., 1998; Schoell, 1984). Diefendorf et al. (2015) found that the catagenic stage of maturation can lead to variations in the magnitude and direction of the change in δ^{13}C-values according to species and chain length. Therefore, the effect of thermal maturation on the δ^{13}C-values measured cannot be ruled out in the present study.

The δ^{13}C-values correspond to common carbon isotope values of C3 plants and freshwater algae (e.g. Close, 2019; Diefendorf and Freimuth, 2017; Holtvoeth et al., 2019; Lamb et al., 2006; Meyers, 1997; O'Leary, 1981). Terrestrial plants utilise atmospheric CO_2 during photosynthesis, whereas aquatic photoautotrophs use dissolved $CO_{2[AQ]}$ or, in the case of alkaline or CO_2-limited conditions, can fix HCO_3^- as the inorganic carbon source for photosynthesis (Holtvoeth et al., 2019; Lamb et al., 2006; Meyers, 1997). The assimilation of HCO_3^- leads to ^{13}C enrichment (Aichner et al., 2010; Lamb et al., 2006; Meyers, 1997). The intermediate-weight *n*-alkanes are isotopically heavier than long-chain *n*-alkanes (Fig. 9), moreover, δ^{13}C isotopic differences could be more explicit prior to the thermal alteration. Furthermore, low-molecular weight *n*-alkanes are characterized by ^{13}C enrichment relative to mid-chain *n*-alkanes (Fig. 9). However, the carbon isotopic composition of lake-derived organic matter is typically indistinguishable from the surrounding watershed (Meyers, 1997). Nevertheless, the contribution of algae to the carbon isotope compositions measured is also suggested by the presence of lamalginite.

The predominance of C_{29} steroids in coals is consistent with a dominant origin of organic matter from vascular plants (Fig. 10; Table 4; Huang and Meinshein, 1979), which also explains the low amount of regular steranes (Doković et al., 2018; Volkman, 1986). Besides the vascular plants, the constant proportion of C_{28} steranes and the occurrence of perylene has been suggested to indicate a contribution from wood-degrading fungi (Marynowski et al., 2013). Hopane derivatives occur in the investigated samples, in which the bacteriohopanepolyols have been suggested to be the most probable biological precursors, and have been identified both in bacteria and in some cryptogams (e.g. moss, ferns; Ourisson et al., 1979; Rohmer, 1993; Talbot et al., 2016). The occurrence of C_{32} to C_{35} benzohopanes (Hussler et al., 1984) in the aromatic hydrocarbon fractions also suggests that bacteriohopanetetrol was a significant constituent of the precursor biomass. Furthermore, both the low sterane to hopane ratio and the presence of drimane-type sesquiterpenoids suggest microbially reworked organic matter (Alexander et al., 1983, 1984; Tissot and Welte, 1984).

Sesquiterpenoids and diterpenoids are present in the analysed sample sets (Table 3). The biological precursors of cadalane-type sesquiterpenoids are widely distributed throughout all conifer families (Simoneit et al., 1986; Otto et al., 1997, and references therein). Eudesmane is also a non-specific indicator of higher land plants (Alexander et al., 1983), hitherto missing in species of Araucariaceae and Taxaceae (Otto and Wilde, 2001). Labdane-type compounds are the most common diterpenoids in conifers and have been described in all families except in Cephalotaxaceae (Otto and Wilde, 2001). More than 100 pimarane- and isopimarane-type diterpenoids have been detected in species of Pinaceae, Taxodiaceae, Araucariaceae, and Cupressaceae (Sukh Dev, 1989). Phyllocladane-type diterpenoids are widespread among coniferales families, except in Pinaceae (Otto and Wilde, 2001). Abietane-type diterpenoids can be generated by the transformation of pimarane (Wakeham et al., 1980), the progressive thermal alteration of phyllocladane (Alexander et al., 1987), or the dehydrogenation of abietic acids (Peters et al., 2005). Alkylated phenanthrenes have been genetically related to abietic- and pimaric acid (Alexander et al., 1995; Laflamme and Hites, 1978; Radke et al., 1998). Based on the composition of diterpenoids present in the studied samples, Cupressaceae genera presumably contributed to the arboreal vegetation.

Non-hopanoid triterpenoids of oleanane-, ursane- and lupane-types are significant constituents of leaf waxes, wood, roots, and bark (Karrer et al., 1977), and the oleanane- and ursane-types are particularly predominant in the samples investigated. These compounds are formed by the transformation of β-amyrin, α-amyrin, and lupeol (Havelcová et al., 2012) and are significant biomarkers of angiosperm inputs into organic matter (Sukh Dev, 1989; Karrer et al., 1977). Aside from non-hopanoid triterpenoids, di- and trimethylnaphthalenes can also originate from angiosperms (van Aarssen et al., 1992; Strachan et al., 1988).

The di-/(di- + triterpenoids) ratio can be used to estimate the relative contribution of gymnosperms and angiosperms to organic matter (Bechtel et al., 2003). Very low ratios (≤0.2; Table 4) indicate that angiosperm-derived biomarkers predominate in all analysed samples of the Kosd Formation. These results are consistent with previous observations on Eocene coal deposits throughout central Europe (Bechtel et al., 2007, 2008) and are supported by palynological data from

throughout the Transdanubian Mountains, which further indicates an angiosperm-dominated vegetation (Kvaček, 2010, and references therein; Rákosi, 1978). Although the vegetation was dominated by angiosperms, a continuous upward increase in the di-/(di- + triterpenoids) ratio from 0.06 to 0.20 (Table 4) indicates an increasing relative contribution of gymnosperms during deposition of the studied depth interval (2602.4–2599.0 m).

5.3. Depositional environment

GWI_{AC} values (> 10) in the studied section suggest that the deposition of the coaly lithotypes occurred in a low-lying mire with rheotrophic conditions (Fig. 6; Table 2; Calder et al., 1991). The presence of inertinite and liptinite in the investigated Kosd coal implies the existence of a paleomire influenced by the fluctuation of the water table (Diessel, 1992; Eble et al., 2019), allowing the accumulation of lamalginite during high-, and the oxidation of plant tissues during low water table conditions.

The *n*-alkane isotope profile shows a generally declining pattern (Fig. 9), which has previously been assigned to fluvio-deltaic origins (e.g. Bjorøy et al., 1991; Cortes et al., 2010; Dzou and Hughes, 1993; Murray et al., 1994; Odden et al., 2002; Tuo et al., 2003; Wilhelms et al., 1994). The Pr/Ph vs. DBT/P plot also indicates a fluvio-deltaic environment (Fig. 11; Hughes et al., 1995). The composition of regular steranes (Fig. 10; Table 4; Huang and Meinshein, 1979) suggests a transition between shallow marine and deltaic paleoenvironments, which provided an appropriate setting for the preservation of higher plant triterpenoids (Strachan et al., 1988).

The sulphur content of the analysed samples has a general tendency towards higher readings with increasing organic carbon content (Table 3). Variations in sulphur content can be explained by an influx of saline water towards the paleomire (Petersen and Ratanasthien, 2011) or by changes in pH (Markič and Sachsenhofer, 1997). Considering the occurrence of marine miliolid foraminifers (Fig. 3c), an influx of marine water is obvious. In addition, the low TOC/TS ratios (Table 1) support marine influence (Berner, 1982, 1984). Denudation of Mesozoic carbonate rocks underlying the Kosd Formation may have enhanced the concentration of bicarbonate ions. Moreover, the chemical weathering in the hinterland provided nutrients to the paleovegetation. Alkaline conditions control both, bacterial decomposition of plant remnants and reduction of sulphates by sulphate-reducing bacteria (Markič and Sachsenhofer, 1997). In the case of available reactive iron, the transformation of sulphide phases into densely packed framboidal aggregates of pyrite crystals is a prevalent process driven by bacterial sulphate reduction (Casagrande, 1987; Hámor, 1994; Maclean et al., 2008; Morad, 1998; Sweeney and Kaplan, 1973). Nevertheless, there is a poor fit between the TS and pyrite contents, which indicates the presence of organic sulphur. Organic sulphur-bearing compounds (e.g. dibenzothiophenes) have been detected in considerable concentrations (Table 3). The prevalence of organic sulphur has also been described for Eocene coals by Hámor-Vidó and Hámor (2007). The marine influence and the presence of mobile Ca^{2+} and HCO_3^- ions in the continental runoff are confirmed by the local elevation of calcite equivalent percentages (at #2, #8, #9, #11 and #33) in the interseam sediments (Table 1).

In the studied samples, Pr and Ph exhibit similar carbon isotopic compositions, and are enriched in ^{13}C relative to terrestrial plant-derived *n*-alkanes, arguing for chlorophyll as their common source (Fig. 9; Collister et al., 1992; Hayes et al., 1990; Hayes, 1993). Confined pyrolysis studies of coal samples support a maturation tendency of Pr/Ph (Monthioux and Landais, 1989; Radke et al., 1980). Therefore, the interpretation of redox conditions during sedimentation based strictly on Pr/Ph ratios (Didyk et al., 1978) is limited in the current study due to interferences resulting from thermal maturity. Nevertheless, the occurrence of des-A-triterpenes suggests dysoxic conditions (Jacob et al., 2007, and references therein). Furthermore, in immature terrigenous organic matter, perylene has been related to the activity of wood-degrading fungi and indicates reducing conditions in subsurface sediments during early diagenesis (Marynowski et al., 2013). Although the studied coals are mature, the presence of framboidal pyrite, as well as perylene, indicates eogenetic origin and locally reducing conditions (Sweeney and Kaplan, 1973).

Whereas Gidai (1978) and Less (2005) have mentioned the presence of coaly layers in wells K–20 and V–75, they did not investigate the organic material. Nevertheless, the new results on well W–1 agree well with the sedimentological and palaeontological data reported by these authors. Despite the strongly varying thickness, all three wells show a general trend from non-marine fine-grained rocks with debris flow deposits to brackish and marine sediments. Coaly layers occur within the transition zone. According to Less (2005), the upper marine part of the Kosd Formation in V–75 represents a lagoonal environment dominated by fine-grained rocks. Based on the lithological and faunal description provided by Gidai (1978), a similar environment can be assumed for well K–20. In contrast, the studied interval in well W–1 includes sandstones and conglomerates representing a delta environment. Moreover, the total thickness of the Kosd Formation in well W–1 (376 m) is higher than in any other well (cf. Less, 2005).

5.4. Hydrocarbon generation potential

The remaining hydrocarbon generation potential of the Kosd Formation samples can be characterized using TOC contents and the amount of free (S1) and generated hydrocarbons (S2). TOC contents of the analysed samples are generally greater than 0.5 wt% (Table 1). The obtained HI values suggest that type III and II–III kerogen is dominant, nevertheless, type IV kerogen also occurs (#12, #16 and #20; Fig. 4a; Table 1). The coaly lithotypes and their adjacent intercalating sediments have excellent and fair-good petroleum potential, respectively (Peters, 1986; Peters and Cassa, 1994). In total, 69% of the analysed samples have HI values between 50 and 200 mg HC/g TOC and are gas-prone, whereas 22% possess oil- and gas-prone kerogen (Peters and Cassa, 1994).

Following the approach of Sykes and Snowdon (2002), coaly samples were plotted onto diagrams of HI, BI and QI versus Tmax (Figs. 4b–d). These diagrams suggest that all coaly samples are gas- and oil-prone (Fig. 4b) and have passed the rank threshold for oil generation (BI; Fig. 4c) and expulsion (QI; Fig. 4d), furthermore, have reached the maturity threshold for the first gas generation (BI; Fig. 4c). Fig. 4c emphasizes the high BI of the coal samples, which is linked to abundant short-chain *n*-alkanes and probably causes the strong fluorescence observed in vitrinite macerals.

6. Conclusion

The investigation of the coal measure of the Eocene Kosd Formation in northern Pannonian Basin has yielded important new results regarding its depositional environment, organic matter source and hydrocarbon potential:

(1) The coal measure evolved in a marine deltaic environment. The accumulation of peat-forming vegetation in a low-lying, rheotrophic mire was affected by fluctuations of the water table.
(2) Slightly alkaline conditions and the depletion in dissolved oxygen noted in the sediments promoted the reduction of sulphates by sulphate-reducing bacteria and bacterial decomposition of plant remains. In addition to the high sulphur contents observed (max. 8.8%), the orange-brown fluorescence colour of vitrinite and its strong swelling during pyrolysis are typical indicators of marine-influenced coals.
(3) The peat-forming flora was dominated by land plants with varying contributions of algae and aquatic macrophytes. Similar to other Eocene coal seams, angiosperms predominated over gymnosperms.

An upward increase in the relative contribution of gymnosperms (e.g. Cupressaceae) to the biomass is observed at depth between 2599.0 and 2604.4 m. The organic matter in the paleomire was highly reworked by microbial processing. Dense flourishing vegetation established a CO_2-limited environment forcing aquatic plants to utilise HCO_3^- during photosynthesis.

(4) Vitrinite reflectance, Tmax, and biomarker indices denote that organic matter in the Kosd Formation (as identified in deep borehole W–1) is thermally mature and suggests that the Kosd coal reached high volatile bituminous rank in the research area. This is higher than the rank of the sub-bituminous coal in the shallow Kosd coalfield of the North Hungarian Mountains. This advanced maturity influenced the molecular and isotopic composition of hydrocarbons.

(5) Rock-Eval pyrolysis results indicate that the coaly samples studied are gas- and oil-prone and have reached the maturity threshold for first gas generation and the onset of oil expulsion.

Declaration of Competing Interest

The authors declare there is no conflict of interest.

Acknowledgement

The authors gratefully acknowledge MOL Plc. for granting the availability of samples and the permission for submitting the manuscript. We thank IJCG's editor-in-chief Professor D. Flores and two anonymous reviewers for their constructive comments. The research was performed during the Ernst Mach scholarship period of SK, supported by 'Aktion Österreich-Ungarn' (ICM-2018-12611). This work was financially sponsored by the University of Szeged Open Access Fund (4665).

References

van Aarssen, B.G.K., Hessels, J.K.C., Abbink, O.A., de Leeuw, J.W., 1992. The occurrence of polycyclic sesqui-, tri-, and oligoterpenoids derived from a resinous polymeric cadinene in crude oils from Southeast Asia. Geochim. Cosmochim. Acta 56, 1231–1246. https://doi.org/10.1016/0016-7037(92)90059-r.

Aichner, B., Herzschuh, U., Wilkes, H., 2010. Influence of aquatic macrophytes on the stable carbon isotopic signatures of sedimentary organic matter in lakes on the Tibetan Plateau. Org. Geochem. 41, 706–718. https://doi.org/10.1016/j.orggeochem.2010.02.002.

Alexander, G., Hazai, I., Grimalt, J., Albaigés, J., 1987. Occurrence and transformation of phyllocladanes in brown coals from Nograd Basin, Hungary. Geochim. Cosmochim. Acta 51, 2065–2073. https://doi.org/10.1016/0016-7037(87)90256-0.

Alexander, R., Kagi, R., Noble, R., 1983. Identification of the bicyclic sesquiterpenes drimane and eudesmane in petroleum. J. Chem. Soc. Chem. Commun. (5), 226–228. https://doi.org/10.1039/c39830000226.

Alexander, R., Kagi, R.I., Noble, R., Volkman, J.K., 1984. Identification of some bicyclic alkanes in petroleum. Org. Geochem. 6, 63–72. https://doi.org/10.1016/0146-6380(84)90027-5.

Alexander, R., Bastow, T.P., Fisher, S.J., Kagi, R.I., 1995. Geosynthesis of organic compounds: II. Methylation of phenanthrene and alkylphenanthrenes. Geochim. Cosmochim. Acta 59, 4259–4266. https://doi.org/10.1016/0016-7037(95)00285-8.

ASTM International, 2015. ASTM D2797/D2797M-11a: Standard Practice for Preparing Coal Samples for Microscopical Analysis by Reflected Light. ASTM International, West Conshohocken, Pennsylvania. https://doi.org/10.1520/d2797_d2797m-11a. (5 p).

ASTM International, 2018. ASTM D3174–12: Standard Test Method for Ash in the Analysis Smple of Coal and Coke from Coal. ASTM International, West Conshohocken, Pennsylvania. https://doi.org/10.1520/d3174-12r18. (6 p).

Badics, B., Vető, I., 2012. Source rocks and petroleum systems in the Hungarian part of the Pannonian Basin: the potential for shale gas and shale oil plays. Mar. Petrol. Geol. 31, 53–69. https://doi.org/10.1016/j.marpetgeo.2011.08.015.

Báldi, T., Báldi-Beke, M., 1985. The evolution of the Hungarian Paleogene Basins. Acta Geol. Hung. 28, 5–28.

Báldi-Beke, M., 2003a. A dunántúli eocén kőszénösszletek fedőképződményeinek rétegtana és paleoökológiája nannoplankton alapján (Stratigraphy and palaeoecology of the formations overlying the Middle Eocene coal sequence based on nannofossils - (Transdanubia, Hungary)). Bull. Hung. Geol. Soc. 133, 325–343 (in Hungarian with English abstract).

Báldi-Beke, M., 2003b. A magyarországi eocén transzgressziók ideje: a nannoplankton biosztratigráfiai és magnetosztratígráfiai eredmények együttes értékelése (Time of the Eocene transgressions in Hungary: evaluation of the nannoplankton biostratigraphy and magnetostratigraphy). Bull. Hung. Geol. Soc. 133, 437–440 (in Hungarian with English abstract).

Bauer, M., M.Tóth, T., Raucsik, B., Garaguly, I., 2016. Petrology and paleokarst features of the Gomba hydrocarbon reservoir (central Hungary). Centr. Eur. Geol. 59, 28–59. https://doi.org/10.1556/24.59.2016.003.

Bechtel, A., Sachsenhofer, R.F., Markic, M., Gratzer, R., Lücke, A., Püttmann, W., 2003. Paleoenvironmental implications from biomarker and stable isotope investigations on the Pliocene Velenje lignite seam (Slovenia). Org. Geochem. 34, 1277–1298. https://doi.org/10.1016/s0146-6380(03)00114-1.

Bechtel, A., Hámor-Vidó, M., Sachsenhofer, R.F., Reischenbacher, D., Gratzer, R., Püttman, W., 2007. The middle Eocene Márkushegy subbituminous coal (Hungary): Paleoenvironmental implications from petrographical and geochemical studies. Int. J. Coal Geol. 72, 33–52. https://doi.org/10.1016/j.coal.2006.12.008.

Bechtel, A., Gratzer, R., Sachsenhofer, R.F., Gusterhuber, J., Lücke, A., Püttmann, W., 2008. Biomarker and carbon isotope variation in coal and fossil wood of Central Europe through the Cenozoic. Palaeogeogr. Palaeoclimatol. Palaeoecol. 262, 166–175. https://doi.org/10.1016/j.palaeo.2008.03.005.

Bechtel, A., Hámor-Vidó, M., Gratzer, R., Sachsenhofer, R.F., Püttmann, W., 2012. Facies evolution and stratigraphic correlation in the early Oligocene Tard Clay of Hungary as revealed by maceral, biomarker and stable isotope composition. Mar. Pet. Geol. 35, 55–74. https://doi.org/10.1016/j.marpetgeo.2012.02.017.

Berner, R.A., 1982. Burial of organic carbon and pyrite sulfur in the modern ocean: its geochemical and environmental significance. Am. J. Sci. 282, 451–473. https://doi.org/10.2475/ajs.282.4.451.

Berner, R.A., 1984. Sedimentary pyrite formation: an update. Geochim. Cosmochim. Acta 48, 605–615. https://doi.org/10.1016/0016-7037(84)90089-9.

Bingham, E.M., McClymont, E.L., Väliranta, M., Mauquoy, D., Roberts, Z., Chambers, F.M., Evershed, R.P., 2010. Conservative composition of n-alkane biomarkers in Sphagnum species: implications for palaeoclimate reconstruction in ombrotrophic peat bogs. Org. Geochem. 41, 214–220. https://doi.org/10.1016/j.orggeochem.2009.06.010.

Bjorøy, M., Hall, K., Gillyon, P., Jumeau, J., 1991. Carbon isotope variations in n-alkanes and isoprenoids of whole oils. Chem. Geol. 93, 13–20. https://doi.org/10.1016/0009-2541(91)90061-u.

Bjorøy, M., Hall, P.B., Hustad, E., Williams, J.A., 1992. Variation in stable carbon isotope ratios of individual hydrocarbons as a function of artificial maturity. Org. Geochem. 19, 89–105. https://doi.org/10.1016/0146-6380(92)90029-w.

Bray, E.E., Evans, E.D., 1961. Distribution of n-paraffins as a clue to recognition of source beds. Geochim. Cosmochim. Acta 22, 2–15. https://doi.org/10.1016/0016-7037(61)90069-2.

Calder, J.H., Gibling, M.R., Mukhopadhyay, P.K., 1991. Peat formation in a Westphalian B piedmont setting, Cumberland basin, Nova Scotia: implications for the maceral-based interpretation of rheotropic and raised paleomires. B. Soc. Geol. Fr. 162, 283–298.

Carr, A.D., 2000. Suppression and retardation of vitrinite reflectance: part 1. Formation and significance for hydrocarbon generation. J. Petrol. Geol. 23, 313–343. https://doi.org/10.1111/j.1747-5457.2000.tb01022.x.

Casagrande, D.J., 1987. Sulphur in peat and coal, in: Scott, a.C. (Ed.), coal and coal-bearing strata: recent advances. Geol. Soc. Lond. Spec. Publ. 32, 87–105. https://doi.org/10.1144/gsl.sp.1987.032.01.07.

Clayton, C.J., 1991. Effect of maturity on carbon isotope ratios of oils and condensates. Org. Geochem. 17, 887–899. https://doi.org/10.1016/0146-6380(91)90030-n.

Close, H.G., 2019. Compound-specific isotope geochemistry in the ocean. Annu. Rev. Mar. Sci. 11, 27–56. https://doi.org/10.1146/annurev-marine-121916-063634.

Collister, J.W., Summons, R.E., Lichtfouse, E., Hayes, J.M., 1992. An isotopic biogeochemical study of the Green River oil shale. Org. Geochem. 19, 265–276. https://doi.org/10.1016/0146-6380(92)90042-v.

Collister, J.W., Lichtfouse, E., Hieshima, G., Hayes, J.M., 1994. Partial resolution of sources of n-alkanes in the saline portion of the Parachute Creek Member, Green River Formation (Piceance Creek Basin, Colorado). Org. Geochem. 21, 645–659. https://doi.org/10.1016/0146-6380(94)90010-8.

Coplen, T.B., 2011. Guidelines and recommended terms for expression of stable-isotope-ratio and gas-ratio measurement results. Rapid Commun. Mass Spec. 25, 2538–2560. https://doi.org/10.1002/rcm.5129.

Cortes, J.E., Rincon, J.M., Jaramillo, J.M., Philp, R.P., Allen, J., 2010. Biomarkers and compound-specific stable carbon isotope of n-alkanes in crude oils from Eastern Llanos Basin, Colombia. J. S. Am. Earth Sci. 29, 198–213. https://doi.org/10.1016/j.jsames.2009.03.010.

Cranwell, P.A., 1977. Organic Geochemistry of Cam Loch (Sutherland) sediments. Chem. Geol. 20, 205–221. https://doi.org/10.1016/0009-2541(77)90044-4.

Cranwell, P.A., Eglinton, G., Robinson, N., 1987. Lipids of aquatic organisms as potential contributors to lacustrine sediments—II. Org. Geochem. 11, 513–527. https://doi.org/10.1016/0146-6380(87)90007-6.

Dehmer, J., 1995. Petrological and organic geochemical investigation of recent peats with known environments of deposition. Int. J. Coal Geol. 28, 111–138. https://doi.org/10.1016/0166-5162(95)00016-x.

Didyk, B.M., Simoneit, B.R.T., Brassell, S.C., Eglinton, G., 1978. Organic geochemical indicators of palaeoenvironmental conditions of sedimentation. Nature 272, 216–222. https://doi.org/10.1038/272216a0.

Diefendorf, A.F., Freimuth, E.J., 2017. Extracting the most from terrestrial plant-derived n-alkyl lipids and their carbon isotopes from the sedimentary record: a review. Org. Geochem. 103, 1–21. https://doi.org/10.1016/j.orggeochem.2016.10.016.

Diefendorf, A.F., Freeman, K.H., Wing, S.L., Graham, H.V., 2011. Production of n-alkyl lipids in living plants and implications for the geologic past. Geochim. Cosmochim. Acta 75, 7472–7485. https://doi.org/10.1016/j.gca.2011.09.028.

Diefendorf, A.F., Sberna, D.T., Taylor, D.W., 2015. Effect of thermal maturation on plant-

derived terpenoids and leaf wax n-alkyl components. Org. Geochem. 89–90, 61–70. https://doi.org/10.1016/j.orggeochem.2015.10.006.
Diessel, C.F.K., 1992. Coal-Bearing Depositional Systems. Springer-Verlag, Berlin.
Doković, N., Mitrović, D., Životić, D., Bechtel, A., Sachsenhofer, R.F., Matić, V., Glamočanin, L., Stojanović, K., 2018. Petrographical and organic geochemical study of the lignite from the Smederevsko Pomoravlje field (Kostolac Basin, Serbia). Int. J. Coal Geol. 195, 139–171. https://doi.org/10.1016/j.coal.2018.06.005.
Dzou, L.I.P., Hughes, W.B., 1993. Geochemistry of oils and condensates, K field, offshore Taiwan: a case study in migration fractionation. Org. Geochem. 20, 437–462. https://doi.org/10.1016/0146-6380(93)90092-p.
Eble, C.F., Greb, S.F., Williams, D.A., Hower, J.C., O'Keefe, J.M.K., 2019. Palynology, organic petrology and geochemistry of the Bell coal bed in Western Kentucky, Eastern Interior (Illinois) Basin, USA. Int. J. Coal Geol. 213, 103264. https://doi.org/10.1016/j.coal.2019.103264.
Eglinton, G., Hamilton, R.J., 1967. Leaf epicuticular waxes. Science 156, 1322–1335. https://doi.org/10.1126/science.156.3780.1322.
Espitalié, J., LaPorte, J.L., Madec, M., Marquis, F., Leplat, P., Paulet, J., Boutefeu, A., 1977. Méthode rapide de charactérisation des roches metres, de leur potential pétrolier et de leur degé d'évolution. Revue de l'Institut Français du Pétrole 32, 23–42. https://doi.org/10.2516/ogst:1977002.
Espitalié, J., Marquis, F., Barsony, I., 1984. Geochemical logging. In: Voorhees, K.J. (Ed.), Analytical Pyrolysis Techniques and Applications, Butterworths, London, pp. 276–304.
Ficken, K.J., Barber, K.E., Eglinton, G., 1998. Lipid biomarker, $\delta^{13}C$ and plant macrofossil stratigraphy of a Scottish montane peat bog over the last two millennia. Org. Geochem. 28, 217–237. https://doi.org/10.1016/s0146-6380(97)00126-5.
Ficken, K.J., Li, B., Swain, D.L., Eglinton, G., 2000. An *n*-alkane proxy for the sedimentary input of submerged/floating freshwater aquatic macrophytes. Org. Geochem. 31, 745–749. https://doi.org/10.1016/s0146-6380(00)00081-4.
Freeman, K.H., Hayes, J.M., Trendel, J.M., Albrecht, P., 1990. Evidence from carbon isotope measurements for diverse origins of sedimentary hydrocarbons. Nature 343, 254–256. https://doi.org/10.1038/343254a0.
Gidai, L., 1978. A kósdi eocén képződmények rétegtani viszonyai (Conditions stratigraphiques des formations éocènes de Kósd). Bull. Hung. Geol. Soc. 108, 65–86 (in Hungarian with extended French summary).
Gross, D., Bechtel, A., Harrington, G.J., 2015. Variability in coal facies as reflected by organic petrological and geochemical data in Cenozoic coal beds offshore Shimokita (Japan) - IODP Exp. 337. Int. J. Coal Geol. 152, 63–79. https://doi.org/10.1016/j.coal.2015.10.007.
Haas, J., Kovács, S., 2012. Pelso composite unit. In: Haas, J. (Ed.), Geology of Hungary. Springer-Verlag, Berlin, pp. 21–81.
Hámor, T., 1994. The occurrence and morphology of sedimentary pyrite. Acta Geol. Hung. 37, 153–181.
Hámor-Vidó, M., Hámor, T., 2007. Sulphur and carbon isotopic composition of power supply coals in the Pannonian Basin, Hungary. Int. J. Coal Geol. 71, 425–427. https://doi.org/10.1016/j.coal.2006.11.002.
Havelcová, M., Sýkorová, I., Trejtnarová, H., Šulc, A., 2012. Identification of organic matter in lignite samples from basins in the Czech Republic: Geochemical and petrographic properties in relation to lithotype. Fuel 99, 129–142. https://doi.org/10.1016/j.fuel.2012.03.025.
Hayes, J.M., 1993. Factors controlling 13C contents of sedimentary organic compounds: principles and evidence. Mar. Geol. 133, 111–126. https://doi.org/10.1016/0025-3227(93)90153-m.
Hayes, J.M., Takigiku, R., Ocampo, R., Callot, H.J., Albrecht, P., 1987. Isotopic compositions and probable origins of organic molecules in the Eocene Messel shale. Nature 329, 48–51. https://doi.org/10.1038/329048a0.
Hayes, J.M., Freeman, K.H., Popp, B.N., Hoham, C.H., 1990. Compound-specific isotopic analyses: a novel tool for reconstruction of ancient biogeochemical processes. Org. Geochem. 16, 1115–1128. https://doi.org/10.1016/0146-6380(90)90147-r.
Holtvoeth, J., Whiteside, J.H., Engels, S., Freitas, F.S., Grice, K., Greenwood, P., Johnson, S., Kendall, I., Lengger, S.K., Lücke, A., Mayr, C., Naafs, B.D.A., Rohrssen, M., Sepúlveda, J., 2019. The paleolimnologist's guide to compound-specific stable isotope analysis – an introduction to principles and applications of CSIA for Quaternary lake sediments. Q. Sci. Rev. 207, 101–133. https://doi.org/10.1016/j.quascirev.2019.01.001.
Horváth, F., Bada, G., Windhoffer, G., Csontos, L., Dövény, P., Fodor, L., Grenerczy, G., Síkhegyi, F., Szafián, P., Székely, B., Tímár, G., Tóth, L., Tóth, T., 2005. Atlas of the Present-Day Geodynamics of the Pannonian Basin: Euroconform Maps with Explanatory Text. http://geophysics.elte.hu/projektek/geodinamikai_atlasz_eng.htm (accessed on 5 August 2019).
Huang, W.Y., Meinshein, W.G., 1979. Sterols as ecological indicators. Geochim. Cosmochim. Acta 43, 739–745. https://doi.org/10.1016/0016-7037(79)90257-6.
Hughes, W.B., Holba, A.G., Dzou, L.I.P., 1995. The ratios of dibenzothiophene to phenanthrene and pristan to phytan as indicators of depositional environment and lithology of petroleum source rocks. Geochim. Cosmochim. Acta 59, 3581–3598. https://doi.org/10.1016/0016-7037(95)00225-o.
Hussler, G., Connan, J., Albrecht, P., 1984. Novel families of tetra- and hexacyclic aromatic hopanoids predominant in carbonate rocks and crude oils. Org. Geochem. 6, 39–49. https://doi.org/10.1016/0146-6380(84)90025-1.
ICCP, 1998. The new vitrinite classification (ICCP System 1994). Fuel 77, 349–358. https://doi.org/10.1016/s0016-2361(98)80024-0.
ICCP, 2001. The new inertinite classification (ICCP System 1994). Fuel 80, 459–471. https://doi.org/10.1016/s0016-2361(00)00102-2.
Jacob, J., Disnar, J.-R., Boussafir, M., Spadano Albuquerque, A.L., Sifeddine, A., Turcq, B., 2007. Contrasted distributions of triterpene derivatives in the sediments of Lake Caçó reflect paleoenvironmental changes during the last 20,000 yrs in NE Brazil. Org. Geochem. 38, 180–197. https://doi.org/10.1016/j.orggeochem.2006.10.007.
Karrer, W., Cherbuliez, E., Eugster, C.H., 1977. Konstitution und Vorkommen der organischen Pflanzenstoffe (exclusive Alkaloide) Ergänzungsband I. Birkhäuser Verlag, Basel und Stuttgart.
Kercsmár, Zs, Budai, T., Csillag, G., Selmeczi, I., Sztanó, O., 2015. Surface Geology of Hungary. Explanatory Notes to the Geological Map of Hungary (1,500 000). Geological and Geophysical Institute of Hungary, Budapest.
Killops, S.D., Funnell, R.H., Suggate, R.P., Sykes, R., Peters, K.E., Walters, C., Woolhouse, A.D., Boudou, J.-P., 1998. Predicting generation and expulsion of paraffinic oil from vitrinite-rich coals. Org. Geochem. 29, 1–21. https://doi.org/10.1016/s0146-6380(98)00087-4.
Kováč, M., Plašienka, D., Soták, J., Vojtko, R., Oszczypko, N., Less, Gy., Ćosović, V., Fügenschuh, B., Králiková, S., 2016. Paleogene palaeogeography and basin evolution of the Western Carpathians, Northern Pannonian domain and adjoining areas. Glob. Planet. Chang. 140, 9–27. https://doi.org/10.1016/j.gloplacha.2016.03.007.
Kubacska, A., 1925. Daten zur Geologie der Umgebung des Nagyszál. Bull. Hung. Geol. Soc. 55, 327–332.
Kvaček, Z., 2010. Forest flora and vegetation of the European early Palaeogene – a review. Bull. Geosci. 85, 63–76. https://doi.org/10.3140/bull.geosci.1146.
Lafargue, E., Marquis, F., Pillot, D., 1998. Rock-Eval 6 applications in hydrocarbon exploration, production, and soil contamination studies. Revue de l'Institut Français du Pétrole 53, 421–437. https://doi.org/10.2516/ogst:1998036.
Laflamme, R.E., Hites, R.A., 1978. The global distribution of polycyclic aromatic hydrocarbons in recent sediments. Geochim. Cosmochim. Acta 42, 289–303. https://doi.org/10.1016/0016-7037(78)90182-5.
Lamb, A.L., Wilson, G.P., Leng, M.J., 2006. A review of coastal palaeoclimate and relative sea-level reconstructions using δ13C and C/N ratios in organic material. Earth-Sci. Rev. 75, 29–57. https://doi.org/10.1016/j.earscirev.2005.10.003.
Less, Gy, 2005. Palaeogene. In: Pelikán, P. (Ed.), Geology of the Bükk Mountains, Explanatory Book of the Geological Map of the Bükk Mountains (1:50 000). Hungarian Geological Society, Budapest, pp. 204–210.
Li, R., Fan, J., Xue, J., Meyers, P.A., 2017. Effects of early diagenesis on molecular distributions and carbon isotopic compositions of leaf wax long chain biomarker *n*-alkanes: Comparison of two one-year-long burial experiments. Org. Geochem. 104, 8–18. https://doi.org/10.1016/j.orggeochem.2016.11.006.
Littke, R., Leythaeuser, D., Radke, M., Schaefer, R.G., 1990. Petroleum generation and migration in coal seams of the Carboniferous Ruhr Basin, Northwest Germany. Org. Geochem. 16, 247–258. https://doi.org/10.1016/0146-6380(90)90045-2.
Lockheart, M.J., Van Bergen, P.F., Evershed, R.P., 1997. Variations in the stable carbon isotope compositions of individual lipids from the leaves of modern angiosperms: implications for the study of higher land plant-derived sedimentary organic matter. Org. Geochem. 26, 137–153. https://doi.org/10.1016/s0146-6380(96)00135-0.
Mackenzie, A.S., Maxwell, J.R., 1981. Assessment of thermal maturation in sedimentary rocks by molecular measurements. In: Brooks, J. (Ed.), Organic Maturation Studies and Fossil Fuel Exploration. Academic Press, London, pp. 239–254.
Mackenzie, A.S., Patience, R.L., Maxwell, J.R., Vandenbroucke, M., Durand, B., 1980. Molecular parameters of maturation in the Toarcian shales, Paris Basin, France–I. changes in the configuration of acyclic isoprenoid alkanes, steranes, and triterpanes. Geochim. Cosmochim. Acta 44, 1709–1721. https://doi.org/10.1016/0016-7037(80)90222-7.
Maclean, L.C.W., Tyliszczak, T., Gilbert, P.U.P.A., Zhou, D., Pray, T.J., Onstott, C., Southam, G., 2008. A high-resolution chemical and structural study of framboidal pyrite formed within a low-temperature bacterial biofilm. Geobiology 6, 471–480. https://doi.org/10.1111/j.1472-4669.2008.00174.x.
Markič, M., Sachsenhofer, R.F., 1997. Petrographic composition and depositional environments of the Pliocene Velenje lignite seam (Slovenia). Int. J. Coal Geol. 33, 229–254. https://doi.org/10.1016/s0166-5162(96)00043-2.
Marynowski, L., Smolarek, J., Bechtel, A., Philippe, M., Kurkiewicz, S., Simoneit, B.R.T., 2013. Perylene as an indicator of conifer fossil wood degradation by wood-degrading fungi. Org. Geochem. 59, 143–151. https://doi.org/10.1016/j.orggeochem.2013.04.006.
Mead, R., Xu, Y., Chong, J., Jaffé, R., 2005. Sediment and soil organic matter source assessment as revealed by the molecular distribution and carbon isotopic composition of n-alkanes. Org. Geochem. 36, 363–370. https://doi.org/10.1016/j.orggeochem.2004.10.003.
Meyers, P.A., 1997. Organic geochemical proxies of paleoceanographic, paleolimnologic, and paleoclimatic processes. Org. Geochem. 27, 213–250. https://doi.org/10.1016/s0146-6380(97)00049-1.
MGSH – Mining and Geological Survey of Hungary, 2019. Digital Coal Cadastre of Hungary. https://map.mbfsz.gov.hu/coal_cadastre/ (accessed on 13 January 2020).
Milota, K., Kovacs, A., Galicz, Z., 1995. Petroleum potential of the North Hungarian Oligocene sediments. Pet. Geosci. 1, 81–87. https://doi.org/10.1144/petgeo.1.1.81.
Monthioux, M., Landais, P., 1989. Natural and artificial maturation of coal: non-hopanoid biomarkers. Chem. Geol. 77, 71–85. https://doi.org/10.1016/0009-2541(89)90017-x.
Morad, S., 1998. Carbonate cementation in sandstones: distribution patterns and geochemical evolution. Sp. Pub. IAS 26, 1–26. https://doi.org/10.1002/9781444304893.ch1.
Murray, A.P., Summons, R.E., Boreham, C.J., Dowling, L.M., 1994. Biomarker and n-alkane isotope profiles for Tertiary oils: relationship to source rock depositional setting. Org. Geochem. 22, 521–542. https://doi.org/10.1016/0146-6380(94)90124-4.
Némedi Varga, Z., 2010. Kőszénföldtan. A magyarországi kőszénelőfordulások áttekintésével és bibliográfiájával. Bíbor kiadó, Miskolc (in Hungarian).
Nott, C.J., Xie, S., Avsejs, L.A., Maddy, D., Chambers, F.M., Evershed, R.P., 2000. N-Alkane distributions in ombrotrophic mires as indicators of vegetation change related

to climate variation. Org. Geochem. 31, 231–235. https://doi.org/10.1016/s0146-6380(99)00153-9.
Nytoft, H.P., Samuel, O.J., Kildahl-Andersen, G., Johansen, J.E., Jones, M., 2009. Novel C15 sesquiterpanes in Niger Delta oils: structural identification and potential application as new markers of angiosperm input in light oils. Org. Geochem. 40, 595–603. https://doi.org/10.1016/j.orggeochem.2009.02.003.
Odden, W., Barth, T., Talbot, M.R., 2002. Compound-specific carbon isotope analysis of natural and artificially generated hydrocarbons in source rocks and petroleum fluids from offshore Mid-Norway. Org. Geochem. 33, 47–65. https://doi.org/10.1016/s0146-6380(01)00127-9.
O'Leary, M.H., 1981. Carbon isotope fractionation in plants. Phytochemistry 20, 553–567. https://doi.org/10.1016/0031-9422(81)85134-5.
Otto, A., Wilde, V., 2001. Sesqui-, di-, and triterpenoids as chemosystematic markers in extant conifers – a review. Bot. Rev. 67, 141–238. https://doi.org/10.1007/bf02858076.
Otto, A., Walther, H., Püttmann, W., 1997. Sesqui- and diterpenoid biomarkers preserved in Taxodium-rich Oligocene oxbow lake clays, Weisselster basin, Germany. Org. Geochem. 26, 105–115. https://doi.org/10.1016/s0146-6380(96)00133-7.
Ourisson, G., Albrecht, P., Rohmer, M., 1979. The hopanoids. Pure Appl. Chem. 51, 709–729.
Ozsvárt, P., Kocsis, L., Nyerges, A., Győri, O., Pálfy, J., 2016. The Eocene-Oligocene climate transition in the Central Paratethys. Palaeogeogr. Palaeoclimatol. Palaeoecol. 459, 471–487. https://doi.org/10.1016/j.palaeo.2016.07.034.
Palotai, M., Csontos, L., 2010. Strike-slip reactivation of a Paleogene to Miocene fold and thrust belt along the central part of the Mid-Hungarian Shear Zone. Geol. Carpath. 61, 4833–4893. https://doi.org/10.2478/v10096-010-0030-3.
Papp, K., 1913. Les ressources houilléres de la Hongrie. In: McInnes, W., Dowling, D.B., Leach, W.W. (Eds.), The Coal Resource of the World. Morang and CO Limited, Toronto.
Pelikán, P., 2005. Mesozoic. In: Pelikán, P. (Ed.), Geology of the Bükk Mountains, Explanatory Book of the Geological Map of the Bükk Mountains (1:50 000). Hungarian Geological Society, Budapest, pp. 187–204.
Pepper, A.S., Corvi, P.J., 1995. Simple kinetic models of petroleum formation. Part I: oil and gas generation from kerogen. Mar. Petrol. Geol. 12, 291–319. https://doi.org/10.1016/0264-8172(95)98381-e.
Peters, K.E., 1986. Guidelines for evaluating petroleum source rocks using programmed pyrolysis. AAPG Bull. 70, 318–329. https://doi.org/10.1306/94885688-1704-11d7-8645000102c1865d.
Peters, K.E., Cassa, M.R., 1994. Applied source rock geochemistry. In: Magoon, L.B., Dow, G.W. (Eds.), The Petroleum System – From Source to Trap. AAPG Mem. 60pp. 93–120 (Tulsa, Oklahoma).
Peters, K.E., Walters, C.C., Moldowan, J.M., 2005. The Biomarker Guide, second ed. Cambridge University Press, Cambridge.
Peters, K.E., Hackley, P.C., Thomas, J.J., Pomerantz, A.E., 2018. Suppression of vitrinite reflectance by bitumen generated from liptinite during hydrous pyrolysis of artificial source rock. Org. Geochem. 125, 220–228. https://doi.org/10.1016/j.orggeochem.2018.09.010.
Petersen, H.I., Ratanasthien, B., 2011. Coal facies in a Cenozoic paralic lignite bed, Krabi Basin, southern Thailand: changing peat-forming conditions related to relative sea-level controlled watertable variations. Int. J. Coal Geol. 87, 2–12. https://doi.org/10.1016/j.coal.2011.04.004.
Pickel, W., Kus, J., Flores, D., Kalaitzidis, S., Christanis, K., Cardott, B., Misz-Kennan, M., Rodrigues, S., Hentschel, A., Hamor-Vido, M., Crosdale, P., Wagner, N., ICCP, 2017. Classification of liptinite – ICCP System 1994. Int. J. Coal Geol. 169, 40–61. https://doi.org/10.1016/j.coal.2016.11.004.
Popov, S.V., Akhmetiev, M.A., Bugrova, E.M., Lopatin, A.V., Amitrov, O.V., Andreeva-Grigorovich, A.S., Zherikhin, V.V., Zaporozhets, N.I., Nikolaeva, I.A., Krasheninnikov, V.A., Kuzmicheva, E.I., Sytchevskaya, E.K., Shcherba, I.G., 2001. Biogeography of the Northern Peri-Tethys from the late Eocene to the early Miocene: part 1. Late Eocene. Paleontol. J. 35, S1–S68 Supp. Ser. 1.
Radke, M., Welte, D.H., 1983. The Methylphenanthrene Index (MPI): A maturity parameter based on aromatic hydrocarbons. In: Bjoroy, M. (Ed.), Advances in Org. Geochem. Wiley, Chichester, pp. 504–512.
Radke, M., Schaefer, R.G., Leythaeuser, D., Teichmüller, M., 1980. Composition of soluble organic matter in coals: relation to rank and liptinite fluorescence. Geochim. Cosmochim. Acta 44, 1787–1800. https://doi.org/10.1016/0016-7037(80)90228-8.
Radke, M., Welte, D.H., Willsch, H., 1982. Geochemical study of a well in the Western Canada Basin: relation of aromatic distribution pattern to maturity of organic matter. Geochim. Cosmochim. Acta 46, 1–10. https://doi.org/10.1016/0016-7037(82)90285-x.
Radke, M., Hilkert, A., Rullkötter, J., 1998. Molecular stable carbon isotope compositions of alkylphenanthrenes in coals and marine shales related to source and maturity. Org. Geochem. 28, 785–795. https://doi.org/10.1016/s0146-6380(98)00048-5.
Rákosi, L., 1978. A magyarországi eocén mangrove palinológiai adatai (Données palynologiques de la mangrove éocène de Hongrie). In: Annual Report of the Hungarian Geological Institute of 1976, pp. 357–374 (in Hungarian with extended French summary).
Rieley, G., Collier, R.J., Jones, D.M., Eglinton, G., Eakin, P.A., Fallick, A.E., 1991. Sources of sedimentary lipids deduced from stable carbon-isotope analyses of individual compounds. Nature 352, 425–427. https://doi.org/10.1038/352425a0.
Rögl, F., 1999. Mediterranean and Paratethys. Facts and hypotheses of an Oligocene to Miocene paleogeography (short overview). Geol. Carpath. 50, 339–349.
Rohmer, M., 1993. The biosynthesis of triterpenoids of the hopane series in the Eubacteria: a mine of new enzymatic reactions. Pure App. Chem. 65, 1293–1298. https://doi.org/10.1351/pac199365061293.
Rooney, M.A., Vuletich, A.K., Griffith, C.E., 1998. Compound-specific isotope analysis as a tool for characterizing mixed oils: an example from the West of Shetlands area. Org. Geochem. 29, 241–254. https://doi.org/10.1016/s0146-6380(98)00136-3.
Sachsenhofer, R.F., Shymanovskyy, V.A., Bechtel, A., Gratzer, R., Horsfield, B., Reischenbacher, D., 2010. Palaeozoic source rocks in the Dniepr–Donets Basin, Ukraine. Pet. Geosci. 16, 377–399. https://doi.org/10.1144/1354-079309-032.
Sachsenhofer, R.F., Popov, S.V., Coric, S., Mayer, J., Misch, D., Morton, M.T., Pupp, M., Rauball, J., Tari, G., 2018. Paratethyan petroleum source rocks: an overview. J. Petrol. Geol. 41, 219–245. https://doi.org/10.1111/jpg.12702.
Schoell, M., 1984. Stable Isotopes in Petroleum Research. In: Advances in Petroleum Geochemistry, pp. 215–245. https://doi.org/10.1016/b978-0-12-032001-1.50009-2.
Schoell, M., Simoneit, B.R.T., Wang, T.G., 1994. Org. Geochem. and coal petrology of tertiary brown coal in the Zhoujing mine, Baise Basin, South China—4. Biomarker sources inferred from stable carbon isotope compositions of individual compounds. Org. Geochem. 21, 713–719. https://doi.org/10.1016/0146-6380(94)90014-0.
Schwarzbauer, J., Littke, R., Meier, R., Strauss, H., 2013. Stable carbon isotope ratios of aliphatic biomarkers in late Palaeozoic coals. Int. J. Coal Geol. 107, 127–140. https://doi.org/10.1016/j.coal.2012.10.001.
Seifert, W.K., Moldowan, J.M., 1986. Use of biological markers in petroleum exploration. In: Johns, R.B. (Ed.), Methods in Geochemistry and Geophysics 24. Elsevier, Amsterdam, pp. 261–290.
Simoneit, B.R.T., Grimalt, J.O., Wang, T.G., Cox, R.E., Hatcher, P.G., Nissenbaum, A., 1986. Cyclic terpenoids of contemporary resinous plant detritus and of fossil woods, amber and coal. Org. Geochem. 10, 877–889. https://doi.org/10.1016/s0146-6380(86)80025-0.
Simoneit, B.R.T., Schoell, M., Stefanova, M., Stojanova, G., Nosyrev, I.E., Goranova, M., 1995. Composition of the extract from a Carboniferous bituminous coal. 2. Compound-specific isotope analyses. Fuel 74, 1194–1199. https://doi.org/10.1016/0016-2361(95)00038-7.
Sofer, Z., 1984. Stable carbon isotope compositions of crude oils: application to source depositional environments and petroleum alteration. AAPG Bull. 68, 31–49. https://doi.org/10.1306/ad460963-16f7-11d7-8645000102c1865d.
Stock, A.T., Littke, R., Lücke, A., Zieger, L., Thielemann, T., 2016. Miocene depositional environment and climate in western Europe: the lignite deposits of the lower Rhine Basin, Germany. Int. J. Coal Geol. 157, 2–18. https://doi.org/10.1016/j.coal.2015.06.009.
Strachan, M.G., Alexander, R., Kagi, R.I., 1988. Trimethylnaphthalenes in crude oils and sediments: effects of source and maturity. Geochim. Cosmochim. Acta 52, 1255–1264. https://doi.org/10.1016/0016-7037(88)90279-7.
Sukh Dev, 1989. Terpenoids. In: Rowe, J.W. (Ed.), Natural Products of Woody Plants. vol. 1. Springer, Berlin, pp. 691–807.
Sweeney, R.E., Kaplan, I.R., 1973. Pyrite framboid formation: laboratory synthesis and marine sediments. Econ. Geol. 68, 618–634. https://doi.org/10.2113/gsecongeo.68.5.618.
Sykes, R., Snowdon, L.R., 2002. Guidelines for assessing the petroleum potential of coaly source rocks using Rock-Eval pyrolysis. Org. Geochem. 33, 1441–1455. https://doi.org/10.1016/s0146-6380(02)00183-3.
Talbot, H.M., McClymont, E.L., Inglis, G.N., Evershed, R.P., Pancost, R.D., 2016. Origin and preservation of bacteriohopanepolyol signatures in Sphagnum peat from Bissendorfer Moor (Germany). Org. Geochem. 97, 95–110. https://doi.org/10.1016/j.orggeochem.2016.04.011.
Tari, G., Báldi, T., Báldi-Beke, M., 1993. Paleogene retroarc flexural basin beneath the Neogene Pannonian Basin: a geodynamic model. Tectonophysics 226, 433–455. https://doi.org/10.1016/0040-1951(93)90131-3.
Taylor, G.H., Teichmüller, M., Davis, A., Diessel, C.F.K., Littke, R., Robert, P., 1998. Organic Petrology. Gebrüder Bontraeger, Berlin.
Tissot, B.T., Welte, D.H., 1984. Petroleum Formation and Occurrences. Springer, Berlin.
Tuo, J., Wang, X., Chen, J., Simoneit, B.R.T., 2003. Aliphatic and diterpenoid hydrocarbons and their individual carbon isotope compositions in coals from the Liaohe Basin, China. Org. Geochem. 34, 1615–1625. https://doi.org/10.1016/j.orggeochem.2003.08.004.
Volkman, J.K., 1986. A review of sterol markers for marine and terrigenous organic matter. Org. Geochem. 9, 83–99. https://doi.org/10.1016/0146-6380(86)90089-6.
Wakeham, S.G., Schaffner, C., Giger, W., 1980. Polycyclic aromatic hydrocarbons in recent lake sediments. II. Compounds derived from biological precursors during early diagenesis. Geochim. Cosmochim. Acta 44, 415–429. https://doi.org/10.1016/0016-7037(80)90041-1.
Wilhelms, A., Larter, S.R., Hall, K., 1994. A comparative study of the stable carbon isotopic composition of crude oil alkanes and associated crude oil asphaltene pyrolysate alkanes. Org. Geochem. 21, 751–759. https://doi.org/10.1016/0146-6380(94)90017-5.
Wilkins, R.V.T., George, S.C., 2002. Coal as a source rock for oil: a review. Int. J. Coal Geol. 50, 317–361. https://doi.org/10.1016/s0166-5162(02)00134-9.